

# Pushing the boundaries of Structure-Based Drug Design through Collaboration with Large Language Models

Bowen Gao <sup>\*1,2</sup> Yanwen Huang <sup>\*3</sup> Yiqiao Liu <sup>3</sup> Wenxuan Xie <sup>4</sup> Wei-Ying Ma <sup>1</sup> Ya-Qin Zhang <sup>1</sup> Yanyan Lan <sup>1</sup>

## Abstract

Structure-Based Drug Design (SBDD) has revolutionized drug discovery by enabling the rational design of molecules for specific protein targets. Despite significant advancements in improving docking scores, advanced 3D-SBDD generative models still face challenges in producing drug-like candidates that meet medicinal chemistry standards and pharmacokinetic requirements. These limitations arise from their inherent focus on molecular interactions, often neglecting critical aspects of drug-likeness. To address these shortcomings, we introduce the Collaborative Intelligence Drug Design (CIDD) framework, which combines the structural precision of 3D-SBDD models with the chemical reasoning capabilities of large language models (LLMs). CIDD begins by generating supporting molecules with 3D-SBDD models and then refines these molecules through LLM-supported modules to enhance drug-likeness and structural reasonability. When evaluated on the CrossDocked2020 dataset, CIDD achieved a remarkable success ratio of 37.94%, significantly outperforming the previous state-of-the-art benchmark of 15.72%. Although improving molecular interactions and drug-likeness is often seen as a trade-off, CIDD uniquely achieves a balanced improvement in both by leveraging the complementary strengths of different models, offering a robust and innovative pathway for designing therapeutically promising drug candidates.

## 1. Introduction

Structure-Based Drug Design (SBDD) is a keystone of modern rational drug discovery paradigm. Recently, various deep generative approaches have been applied in this field and have gained great advancements, enabling the direct generation of molecules for a given protein/pocket structure. Autoregressive models, such as AR (Luo et al., 2021) and Pocket2Mol (Peng et al., 2022), iteratively construct molecules by sequentially adding atoms to existing structures. While non-autoregressive generative models, including diffusion-based approaches like TargetDiff (Guan et al., 2023) and DecompDiff (Guan et al., 2024), as well as Bayesian flow network-based models such as MolCRAFT (Qu et al., 2024), progressively decrease the noise from a provided random distribution to generate new molecules.

Current 3D-SBDD models often achieve favorable docking scores by relying on distorted substructures, such as unconventional polycyclic systems or unreasonable ring formations, to fit target pockets. However, these distortions compromise molecular stability and reduce drug-likeness properties, such as aqueous solubility and oral absorption. As shown in Figure 1, introducing common SBDD errors into the rationally designed drug Imatinib results in substantial 3D conformational changes despite minimal 2D alterations. Correcting these distortions often disrupts the overall 3D structure, compromising binding affinity. This trade-off between structural accuracy and binding performance limits the practical utility of current 3D-SBDD models.

Addressing this issue within the existing SBDD framework is challenging due to the limitations of reconstruction objective. Specifically, current SBDD models focus on learning the distribution of  $p(\text{molecule} \mid \text{target})$  from protein-ligand complex data, enabling the generation of molecules that exhibit rational structural bindings with the given targets. However, a significant gap remains between these molecules and their potential to be viable drugs, as they must also account for numerous complex factors, such as chemical reasonability, aqueous solubility, lipophilicity, binding affinity, pharmacokinetics, and more. These characteristics are clearly not easily captured through a conditional distribution  $p(\text{molecule} \mid \text{target})$ . Even if we can model them in

<sup>\*</sup>Equal contribution <sup>1</sup>Institute for AI Industry Research (AIR), Tsinghua University. <sup>2</sup>Department of Computer Science and Technology, Tsinghua University. <sup>3</sup>Department of Pharmaceutical Science, Peking University. <sup>4</sup>School of Future Technology, South China University of Technology.. Correspondence to: Yanyan Lan <lanyanyan@air.tsinghua.edu.cn>.

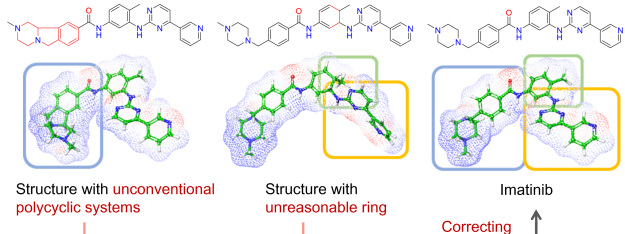


**Figure 1. Two Common Errors in Current 3D-SBDD Model Outputs.** Distorted 3D substructures and their corresponding correct 3D conformations in the accurate structure are marked by boxes.

a single distribution  $p(\text{drug})$ , which presents its own set of challenges, integrating both distributions into a unified framework for learning remains a complex task. As a result, solving this problem using SBDD models alone proves to be insufficient.

The recent emergence of large language models (LLMs) has led to significant breakthroughs across various scientific domains, including protein structure prediction (Valentini et al., 2023), mathematical reasoning (Ahn et al., 2024), code generation (Hong et al., 2023), and medical question answering (Liévin et al., 2024). These models leverage vast amounts of scientific literature, integrating a broad array of scientific knowledge, and have proven exceptionally effective in tackling complex scientific challenges. In drug discovery, for instance, models like GPT-4 have demonstrated impressive abilities in generating molecules with drug-likeness properties, achieving a 97.5% “reasonability” ratio compared to traditional SBDD models. Despite these promising results, LLMs face a critical limitation: they struggle to model the precise spatial arrangement of atomic coordinates in protein binding pockets. As a result, while these molecules may exhibit favorable drug-like characteristics, their binding affinities often fall short.

Inspired by these advances and the multifaceted challenges inherent in drug discovery, we propose a novel Collaborative Intelligence approach for drug design, termed CIDD. This approach combines the complementary strengths of 3D-SBDD models and LLMs to bridge the gap between binding affinity and molecular reasonability, ultimately enabling the generation of more effective drug candidates.

The process begins with 3D-SBDD models generating initial supporting molecules, which are refined through a streamlined pipeline consisting of several LLM-powered modules. An interaction analysis module identifies key molecular fragments contributing to crucial interactions with the protein pocket. A design module detects uncommon or suboptimal structures within the molecule and proposes modifications to enhance drug-likeness while preserving essential inter-

actions. A reflection module evaluates prior designs, highlighting strengths and weaknesses to inform future designs. This cycle repeats multiple times to generate a variety of designs, which are then evaluated in a selection module to identify the optimal molecule balancing interaction capability and drug-likeness properties. By synergizing the structural interaction insights of SBDD with the extensive chemical expertise of LLMs, this framework enables the creation of molecules that excel in both target binding and human-preferred drug-like qualities.

We evaluate the performance of the CIDD framework on the CrossDocked2020 dataset (Francoeur et al., 2020), benchmarking it against several state-of-the-art (SOTA) 3D-SBDD models. The results show that CIDD outperforms these models across multiple metrics, significantly improving both interaction capabilities and drug-likeness. Specifically, the CIDD framework increases the success ratio from 15.72% to 37.94%, and achieves an up to 16.3% improvement in Docking Score, a 20.0% boost in Synthetic Accessibility (SA) Score, an 85.2% rise in Reasonable Ratio, and a 102.8% increase in the ratio of molecules meeting multiple property requirements. These results highlight the ability of CIDD to optimize key molecular properties, particularly binding affinity and drug-likeness, underscoring its potential as a transformative tool in drug discovery. The CIDD framework integrates LLMs with human expertise, computational tools, and advanced models to accelerate pharmaceutical innovation. Focused on refining molecules from SBDD, CIDD can also be applied to target identification, toxicity prediction, and molecular synthesis, combining LLM knowledge with human judgment to optimize drug discovery and move toward an automated, explainable system for medicinal chemists.

## 2. Preliminaries

### 2.1. Structure-Based Drug Design

The goal of SBDD is to generate a molecule  $x$  that can bind to a given protein pocket  $P$ . Recently, the development of SBDD models has shifted towards deep generative models. Autoregressive models, such as AR (Luo et al., 2021) and Pocket2Mol (Peng et al., 2022), generate molecules by sequentially adding new atoms to the existing structure. Subsequently, non-autoregressive generative models have emerged, including diffusion-based models like TargetDiff (Guan et al., 2023) and DecompDiff (Guan et al., 2024), as well as Bayesian flow network-based models like MolCRAFT (Qu et al., 2024).

### 2.2. Large Language Models

LLMs are advanced neural networks trained on vast corpora of textual data, enabling them to understand, generate, and

process human-like language. Notable examples include GPT-4 (Achiam et al., 2023), LLaMA (Touvron et al., 2023), ChatGLM (GLM et al., 2024), and DeepSeek (Liu et al., 2024), which have demonstrated remarkable performance in tasks such as natural language understanding, code generation, mathematical problem solving, and logical reasoning. Their versatility and ability to learn complex patterns have made them increasingly relevant in domains beyond traditional natural language processing, including drug discovery (Chakraborty et al., 2023).

Despite their potential, applying LLMs to structure-based drug design presents unique challenges. Protein structures are not purely textual but are spatially complex, involving three-dimensional arrangements of atoms and intricate chemical interactions. Representing these structural features in a form that LLMs can effectively process is a non-trivial task.

### 3. Methods

#### 3.1. New Metric Design

Drug discovery and development (DDD) is shaped by numerous human factors, including subjective preferences for molecular structures and the complexity of specific tasks. These factors are deeply rooted in implicit or tacit knowledge. However, this does not imply that human perceptions of “drug-likeness” are indescribable or that  $p(\text{drug})$  can simply be bent to match the output distributions of current molecular generative models.

As highlighted in the preceding section, molecules generated by current SBDD models often diverge significantly from real drugs, particularly in the conjugation patterns of their ring systems. To capture this divergence, we developed two rule-based metrics—the Molecular Reasonability Ratio (MRR) and the Atom Unreasonability Ratio (AUR)—to assess “drug-likeness”, focusing on whether aromaticity is preserved in the examined molecules. Aromaticity, a fundamental concept in medicinal chemistry, describes the unique stability and electronic structure of certain ring systems, such as benzene. As a key feature of many Food and Drug Administration (FDA)-approved drugs, these structures are not only chemically stable but also essential for drug-target interactions, facilitating strong binding through mechanisms like  $\pi$ - $\pi$  stacking and hydrophobic interactions. However, current AI-driven generative models for SBDD often fail to replicate the nuanced use of aromatic rings observed in expert-designed molecules. These deviations lead to AI-generated molecules that significantly differ from clinically relevant drugs. By addressing this gap, MRR and AUR aim to better align AI-generated outputs with the practical and structural requirements of drug discovery.

**Molecular Reasonability Ratio.** The Molecular Reasonability metric evaluates the chemical plausibility of a molecule by analyzing its ring systems. Rings sharing one or more atoms are grouped into the same ring system, excluding carbonyl and imine groups. Each ring is evaluated to determine whether it forms an aromatic conjugated structure or a fully saturated ring. Rings meeting these criteria have their constituent atoms removed from further analysis. This process continues iteratively until no additional rings meet the criteria. If no ring atom(s) remain, the molecule is deemed reasonable; otherwise, it is considered unreasonable. Then for all molecules, we calculate the MRR. The full algorithm for MRR calculation is in Appendix B.

**Atom Unreasonability Ratio.** The Atom-level Unreasonable is calculated as the number of atoms in the remaining rings that did not meet the criteria during the iterative process divided by the total number of atoms in all ring systems of the molecule under evaluation. This metric is averaged across all molecules, yielding the AUR.

These metrics provide practical and interpretable indicators of “drug-likeness” from a structural perspective. By incorporating these metrics, AI-driven generative models can produce outputs that better align with real-world medicinal chemistry requirements. By focusing on key structural features such as ring systems, these metrics ensure that generated compounds not only meet computational criteria but also resonate with the empirical knowledge and intuitive preferences of human experts—a critical consideration for successful drug discovery.

**QikProp Multiple Property Requirements.** To further evaluate the physicochemical and pharmacokinetic properties of the generated molecules, we employ QikProp, a tool recognized for its robust performance in predicting molecular drug-likeness properties (Ioakimidis et al., 2008). The assessed properties include aqueous solubility, lipophilicity, polar surface area (PSA), the number of metabolizable sites, and oral absorption. Detailed requirements for each property are provided in Appendix C.

A molecule is considered to have passed the evaluation if it satisfies all  $N$  predefined property requirements:  $P_1, P_2, \dots, P_N$ . If any of the properties fall outside the acceptable range, the molecule is classified as failing.

$$\text{QikProp} = \begin{cases} 1 & \text{if } P_1 \wedge P_2 \wedge \dots \wedge P_N \text{ are satisfied,} \\ 0 & \text{otherwise.} \end{cases}$$

#### 3.2. CIDD Framework

We propose the CIDD framework, illustrated in Figure 2, which integrates advanced computational techniques to advance the field of structure-based drug design. At its core

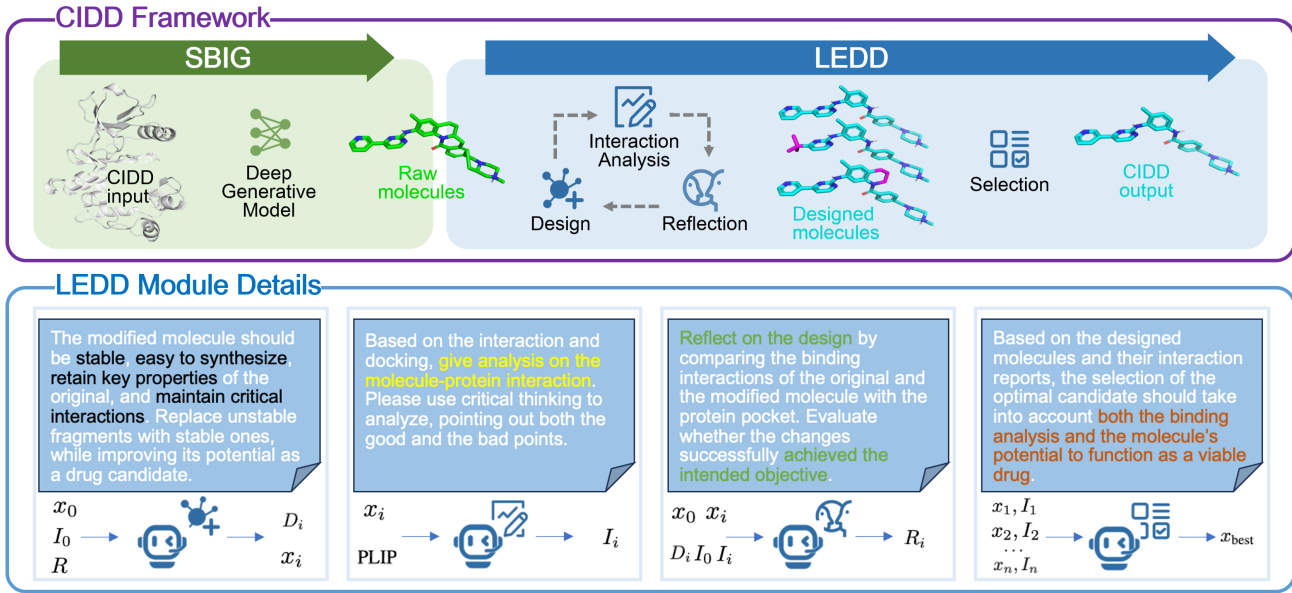


**Figure 2. The CIDD Framework.** The framework comprises two main steps. First, the **Structure-Based Interaction Generator (SBIG)** generates a supporting molecule  $x_0$  and its corresponding interaction report  $I_0$ . The second step, the **LLM-Enhanced Drug Designer (LEDD)**, refines the initial molecule. Using previous reflections  $R = \{R_1, R_2, \dots, R_n\}$ , the LEDD step produces a series of generated designs  $D_i$ , with corresponding designed molecules  $X_i$  and interaction reports  $I_i$ . Finally, the selection module identifies the best-designed molecule, denoted as  $x_{best}$ . The prompts for each modules are also shown, with key words highlighted.

lies the **Structure-Based Interaction Generator (SBIG)** step, which leverages 3D-SBDD models. These models excel at identifying and modeling interactions between protein pockets and small molecules, generating initial molecular proposals that adhere to the structural and chemical constraints of the target.

Following this initial step, the system employs a multi-module refinement process powered by LLMs, referred to as the **LLM-Enhanced Drug Designer (LEDD)**. This component is designed to transform the raw supporting molecular candidates into optimized drug-like compounds tailored to specific targets. By combining the detailed interaction capabilities of SBIG with the broad contextual knowledge of LEDD, the CIDD framework enables a transition from interaction-driven molecule design to comprehensive drug design.

The central objective of the LEDD component is to maintain the interaction capabilities of the original molecule while enhancing its drug-likeness. This transformation is modeled as a conditional distribution:

$$x \sim P(\text{Drug} \mid x_0, \text{Target}),$$

where  $x_0$  represents the raw supporting molecule generated by SBIG, *Target* is the protein pocket or biological target, and  $x$  is the refined drug-like compound. This probabilistic framework captures the refinement process, where initial molecular proposals are optimized into viable drug candi-

dates designed for their specific targets.

A key challenge in this transformation lies in the lack of pairwise data linking unoptimized molecules to their drug-like counterparts. LLMs are particularly well-suited to address this challenge, as they are trained on extensive corpora of scientific literature and unstructured data. This training equips them with a nuanced understanding of chemical properties, preferred fragments, and drug-likeness criteria. By leveraging this knowledge, LLMs facilitate the generation of refined molecular structures that align with both target interaction requirements and drug development principles.

The integration of 3D-SBDD models and LLMs is a defining feature of the CIDD framework. While 3D models generate structurally sound initial proposals by focusing on interaction fidelity, LLMs improve these molecules by optimizing properties such as stability, solubility, and bioavailability. This complementary approach results in a coherent system that combines the strengths of both methodologies to advance the process of drug discovery.

The subsequent sections detail the complete pipeline of the CIDD framework and provide a thorough explanation of its modular components. This includes an examination of the interplay between SBIG and LLM-driven refinement, which underscores the potential of the CIDD system in addressing challenges in drug design.

### 3.2.1. PIPELINE

The supporting molecules generated by the SBIG module are first processed by the **Interaction Analysis Module**, which produces a detailed interaction report outlining their binding characteristics with the target protein. This report, along with the initial supporting molecule, is then provided to the **Design Module**. The Design Module formulates improvement strategies based on the analysis of the supporting molecule and the interaction report, and applies these strategies to refine the molecule, resulting in a new, optimized version. The refined molecule is subsequently reanalyzed by the Interaction Analysis Module to assess its updated interaction properties.

The **Reflection Module** then takes the initial supporting molecule, the design steps, the modified molecule, and the interaction reports to evaluate whether the design has achieved its objectives. This process is repeated over  $N$  rounds, with each round generating a new design proposal starting from the supporting molecule. Importantly, the reflections from previous rounds are used as guidance to inform and refine the design steps in subsequent rounds.

Finally, the **Selection Module** evaluates all designed molecules and their corresponding interaction reports to select the best design that balances interaction quality and drug-likeness.

### 3.2.2. MODULE DETAILS

**Interaction Analysis.** The **Interaction Analysis Module** evaluates the binding interactions between a molecule and the target protein pocket. Its input is a molecule, and its output is a detailed interaction report. The process is as follows: 1. Dock the molecule into the protein pocket. 2. Decompose the molecule into fragments using Breaking of Retrosynthetically Interesting Chemical Substructures (BRICS) (Degen et al., 2008). 3. Use Protein–Ligand Interaction Profiler (PLIP) (Salentin et al., 2015) to identify all Non-Covalent Interactions between the molecule and the protein pocket. 4. Analyze the interaction results using an interaction-specific Large Language Model ( $LLM_I$ ) to match each fragment to its interactions and assess their contributions. The process can be expressed as:

$$LLM_I(PLIP(Docking(x_i, P))) \rightarrow I_i$$

Here,  $x_i$  is the molecule,  $P$  is the target protein pocket, and  $I_i$  is the interaction report generated by  $LLM_I$ .

**Design.** The **Design Module** refines the supporting molecule  $x_0$  by proposing modifications based on its interaction report  $I_0$  and prior reflections  $R = \{R_1, R_2, \dots, R_n\}$ . A design-specific Large Language Model ( $LLM_D$ ) formulates these design steps to enhance drug-likeness while maintaining the molecule’s binding efficacy. This process is

expressed as:

$$LLM_D(x_0, I_0, R) \rightarrow D_i, x_i$$

Here,  $D_i$  represents the design steps proposed by  $LLM_D$ , and  $x_i$  is the modified molecule.

**Reflection.** The **Reflection Module** evaluates the design process by analyzing the initial molecule  $x_0$ , the design  $D_i$ , the refined molecule  $x_i$ , and the interaction report  $I_0$  and  $I_i$ . A reflection-specific Large Language Model ( $LLM_R$ ) provides feedback for future iterations. This process is expressed as:

$$LLM_R(x_0, I_0, D_i, x_i, I_i) \rightarrow R_i$$

Here,  $R_i$  is the feedback output generated by  $LLM_R$ , used to improve subsequent design cycles.

**Selection.** The **Selection Module** evaluates all refined molecules  $x_1, x_2, \dots, x_n$  and their interaction reports  $I_1, I_2, \dots, I_n$ . A selection-specific Large Language Model ( $LLM_S$ ) determines the best candidate by balancing interaction quality and drug-likeness. The process can be expressed as:

$$LLM_S(\{x_1, I_1\}, \{x_2, I_2\}, \dots, \{x_n, I_n\}) \rightarrow x_{best}$$

Here,  $x_{best}$  is the optimal drug candidate selected by  $LLM_S$ .

As shown in Figure 2, we use domain-knowledge guided prompts to enable LLMs to rationally modify the molecules. All the detailed prompts and example responses for those modules are shown in Appendix A.

## 4. Experiments

### 4.1. Experiment Settings

**Dataset.** Following the setup of previous 3D-SBDD models, we utilized the CrossDocked2020 dataset (Francoeur et al., 2020) as our primary resource, and use the same splitting and testing setting as in TargetDiff (Guan et al., 2023) that leads to 100 protein pockets for testing.

**Metrics.** For evaluation, we adopted conventional metrics, including Vina docking score (Trott & Olson, 2010) to assess the binding affinity of molecules, Quantitative Estimate of Drug-likeness (QED) score (Bickerton et al., 2012) to quantitatively evaluate drug-likeness, and SA score (Ertl & Schuffenhauer, 2009) to assess the synthetic feasibility of molecules. Additionally, molecular diversity was considered to measure the structural variability of the generated compounds, which is calculated by 1 - Extended-Connectivity Fingerprints 4 (ECFP4) similarity (Rogers & Hahn, 2010).

Beyond these conventional metrics, we introduced a stronger focus on assessing the drug potential of molecules

using novel metrics such as the MRR and AUR. These metrics provide deeper insights into molecular plausibility and atom-level chemical validity. Furthermore, we incorporated the QikProp pass ratio to refine the evaluation of drug-likeness, ensuring that the generated molecules meet critical physicochemical and pharmacokinetic criteria.

We also included the success ratio, as defined in previous studies, where success is determined by satisfying the criteria: Vina docking score  $< -8.18$ , QED  $> 0.25$ , and SA  $> 0.59$ , as proposed by Long et al. (2022). Additionally, we use the proposed reasonability defined in section 3.1 as an additional criterion for a molecule to be considered successful.

**Baseline Models.** We compared our CIDD method with several classic 3D-SBDD models, including the autoregressive models like AR and Pocket2Mol, diffusion-based models such as TargetDiff and DecompDiff, and the Bayesian flow network-based model MolCRAFT.

**CIDD Settings.** We utilize DecompDiff for the SBIG step. For the LEDD step, all modules are powered by GPT-4o. The Design Module operates for 5 rounds ( $N = 5$ ), generating 5 molecular candidates for the Selection Module, which then identifies the most optimal molecule. For each protein pockets, we generate 10 molecules. All the models used in SBIG step are trained with the CrossDocked2020 dataset and we use their released model weights.

## 4.2. General Results

The general benchmark results including CIDD and other 3D-SBDD models are shown in Table 1.

The presented CIDD utilizes the diffusion-based model DecompDiff to generate initial molecular proposals, which are then refined using our collaborative large language model system to enhance drug-likeness while maintaining interaction specificity. As shown in Table 1, CIDD outperforms conventional SBDD models, achieving an outstanding Vina docking score. It also surpasses all 3D-SBDD models in key druglikeness metrics, including MRR, AUR, and QikProp pass ratios. While CIDD slightly lags behind Pocket2Mol in QED and SA scores, its docking score far surpasses that of Pocket2Mol. This highlights the ability of CIDD to generate molecules that not only exhibit strong interaction potential but are also drug-like and synthetically feasible. CIDD significantly outperforms other methods in terms of success ratio, achieving **37.94%** compared to **15.72%** for the best alternative. This success ratio, which considers **docking score, synthetic feasibility, drug-likeness, and structural reasonability** together, highlights CIDD’s ability to overcome a key limitation of conventional **3D structure-based drug design (SBDD)** models—their difficulty in generating

drug-like molecules. As a result, CIDD successfully facilitates the transition from **structure-based molecule design to structure-based drug design**, achieving our initial goal.

## 4.3. Improvements with Different Models

The proposed CIDD framework is a flexible and plug-and-play solution that enhances various 3D SBDD models by generating improved initial molecules. Figure 3 demonstrates the impact of CIDD across four key metrics: Docking Score (interaction quality), SA Score (synthetic accessibility), Reasonable Ratio (chemical fesibility), and QikProp Pass Ratio (general molecular properties). The lighter-shaded bars represent the baseline models, while the darker-shaded bars show performance after incorporating CIDD, with percentage improvements indicated between them. CIDD consistently enhances all metrics across models, achieving significant gains such as up to 16.3% in Docking Score, 20.0% in SA Score, 85.2% in Reasonable Ratio, and 102.8% in QikProp Pass Ratio. These results highlight the ability of CIDD to adapt and improve diverse SBDD models, particularly excelling in drug-likeness and molecular property optimizations, making it a robust and effective framework for drug discovery.

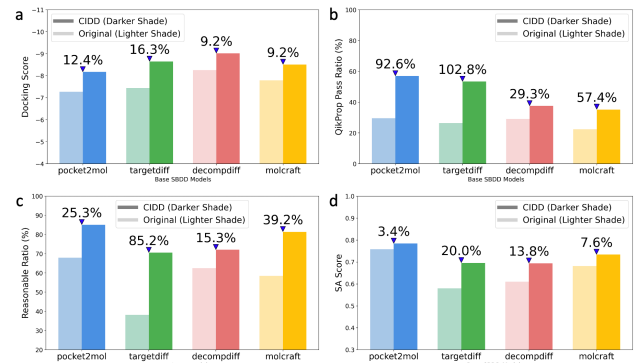


**Figure 3. Comparative Results:** (a) Docking Scores, (b) QikProp Ratios, (c) Molecule Reasonable Ratios, and (d) SA Scores before (*lighter color*) and after (*darker color*) applying the CIDD framework with different 3D-SBDD models.

## 4.4. Ablation and Analysis

### 4.4.1. DIFFERENT LLMs

For the CIDD results shown in Table 1 and Figure 3, the Large Language Model we used is **GPT-4o** from OpenAI. Here, we also test and compare different LLMs, including **GPT-4o-mini**, **GPT-4o**, and the recently released **DeepSeek-v3** (DeepSeek-AI et al., 2024) and **DeepSeek-r1** (Guo et al., 2025). The base SBDD model used in these tests is **MolCRAFT**.

**Table 1. Test Results on CrossDocked2020:** The best results are highlighted in **bold**, while the second-best results are indicated with underline.

Method	Vina ↓	QED ↑	SA score ↑	MRR ↑	AUR ↓	Success Ratio ↑	QikProp ↑	Diversity ↑
AR	-6.737	0.507	0.635	<b>56.67%</b>	34.72%	3.28%	18.66%	0.836
Pocket2Mol	-7.246	<b>0.573</b>	<b>0.758</b>	<u>67.88%</u>	<u>20.14%</u>	14.60%	<u>29.58%</u>	0.866
TargetDiff	-7.452	0.474	0.579	37.81%	43.40%	3.04%	27.63%	<b>0.890</b>
DecompDiff	<u>-8.260</u>	0.444	0.609	62.60%	21.76%	<u>15.72%</u>	29.04%	<u>0.877</u>
MolCRAFT	-7.783	0.503	0.685	58.47%	25.59%	13.72%	22.37%	0.870
CIDD	<b>-9.019</b>	<u>0.525</u>	0.694	<b>76.54%</b>	<b>11.44%</b>	<b>37.94%</b>	<b>37.54%</b>	0.870

The test results, presented in Table 2, demonstrate that all tested LLMs effectively enhance the performance of the CIDD framework compared to using the base SBDD models alone. For metrics such as **MRR** and **QikProp**, which indicate drug-likeness, the LLMs show minimal differences. However, **GPT-4o**, **DeepSeek-v3** and **DeepSeek-r1** exhibit superior performance in improving docking scores, reflecting their enhanced ability to understand molecular interactions. Interestingly, the LLMs display notable variation in the similarity between the raw molecules proposed by the base SBDD models and the final modified molecules produced by CIDD. Since our goal is to minimize molecular modifications while improving properties, high similarity is preferred. This suggests that **GPT-4o-mini** may lack the ability to make subtle, targeted adjustments to molecular structures, whereas **DeepSeek-v3** emerges as the best performer, achieving property improvements with minimal modifications to the original molecules. Surprisingly, DeepSeek-r1 did not achieve better similarity metrics compared to v3, despite its superior performance in math problem-solving and complex reasoning tasks. We attribute this to the nature of our pipeline, which are more domain knowledge-driven rather than requiring complex reasoning. Furthermore, the results demonstrate that by leveraging models like GPT-4o and DeepSeek-v3, we can generate **a substantial amount of high-similarity pairwise data**, where one molecule exhibits improved properties over the other, as discussed in the previous section.

**Table 2. Ablation results for using different LLMs.**

LLM	Vina↓	MRR↑	QikProp↑	Similarity↑
-	-7.78	58.47%	22.37%	-
GPT-4o-mini	-8.29	80.02%	36.43%	0.220
GPT-4o	-8.50	81.37%	35.22%	0.296
DeepSeek-v3	-8.49	76.00%	34.13%	0.379
DeepSeek-r1	-8.57	79.17%	36.72%	0.182

#### 4.4.2. NUMBER OF DESIGNS

An important hyperparameter in CIDD is the number of proposed designs ( $N$ ). To evaluate its impact, we conduct experiments with varying values of  $N$ . As illustrated in Figure 5, the x-axis represents the number of designs, while the y-axis displays the Vina docking score and the MRR. Dashed lines indicate the corresponding values for the original supporting molecules. When  $N = 1$ , the average docking score is slightly worse than that of the supporting molecules. However, the molecular reasonability ratio already shows a significant improvement. As  $N$  increases, the docking score improves progressively, although the MRR experiences a slight decline. At  $N = 5$ , a favorable balance is achieved, with both the average docking score and MRR better than the original supporting molecules.

#### 4.4.3. USING PURE LLM FOR GENERATIONS

**Table 3. Ablation study of using pure LLM for SBDD.**

	Vina↓	MRR↑	Diversity↑	Success Ratio↑
LLM-SBDD	-6.244	97.45%	0.808	5.95%
CIDD-LLM	-7.230	90.97%	0.830	17.59%
CIDD	-9.019	76.54%	0.870	37.94%

As previously discussed, using pure LLMs for structure-based drug design is challenging due to their inability to comprehend the complex three-dimensional structure of protein pockets. To validate this, we conducted a test by providing the pocket structure in PDB format to the LLM and instructing it to generate molecules capable of binding to the target. This approach is referred to as LLM-SBDD. Additionally, we integrated the LLM-SBDD into the CIDD framework, using the LLM-SBDD for the SBIG step. This variant is referred to as CIDD-LLM.

As shown in Table 3, LLM-SBDD generates molecules with a very high reasonability ratio, supporting our motivation for using LLMs to refine supporting molecules into drug candidates. However, LLM-SBDD produces molecules with poor

## CIDD: Collaborative Intelligence Drug Design

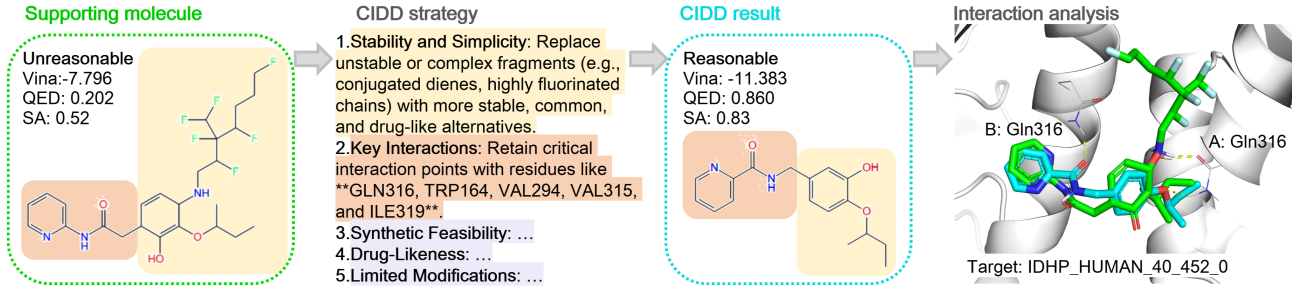


Figure 4. Generation Case and Corresponding Design Strategy Produced by CIDD.

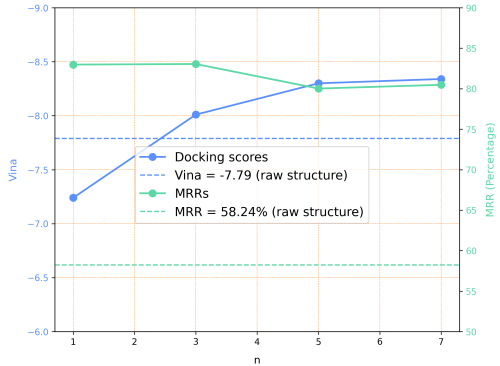


Figure 5. Ablation Study on the Number of Designs: The x-axis represents  $n$ , the number of designs. The blue line corresponds to **Vina docking scores**, while the green line represents **Molecule Reasonable Ratios**. Dashed lines indicate the values for the initial supporting molecule generated by the 3D-SBDD model.

Vina docking scores, resulting in a low overall success ratio compared to the standard CIDD, which utilizes DecompDiff as the SBIG step. These results highlight the critical importance of collaborative intelligence, leveraging both the 3D-SBDD models for their ability to construct interactions and LLMs for their extensive chemical knowledge.

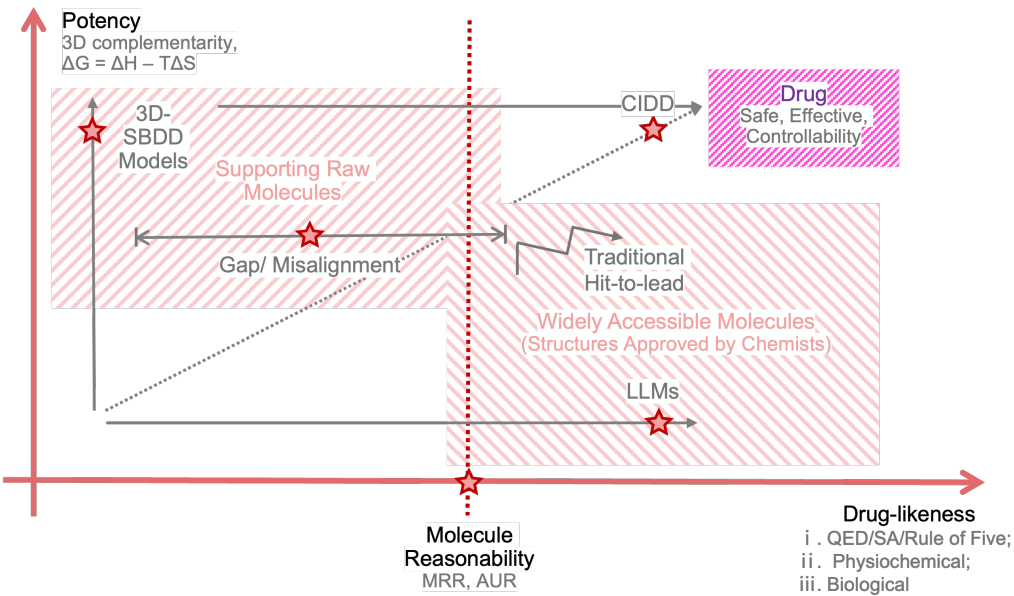
### 4.5. Analysis of Generated Molecules

Figure 4 illustrates the CIDD generation process. The LLM-powered modules within the CIDD framework analyzed and refined the raw supporting molecule (green), resulting in a high-quality final structure (blue). The modules automatically detected issues in the supporting molecule, such as an unreasonable diene substructure, which was replaced with a benzene ring, and an uncommon fluorinated chain, which was modified accordingly. Additionally, side chains were optimized to maintain hydrogen bonding with Gln316 on both Chain A and B of the target protein, improving the original docking score as planned while enhancing the overall drug-likeness properties. This also demonstrates

another advantage of our method: **the design process is explainable**. CIDD not only generates optimized molecules but also provides insights into the rationale behind its design, highlighting structure strengths and potential areas for improvement. This transforms traditional opaque SBDD into an explainable and interpretable approach, making it more beneficial for human experts in drug discovery.

As demonstrated by the visualizations and the prior ablation study, there is a high degree of similarity between the initial raw molecule and the fine-grained molecule generated by CIDD. These modifications are controllable, as they primarily involve substituting unreasonable fragments with reasonable counterparts, rather than transforming the entire molecule into something entirely different. This provides significant advantages from a **data-centric perspective**. This approach enables the **automatic generation of extensive pairwise data**, where one molecule is a refined version of another, exhibiting enhanced drug-likeness properties. Such data inherently captures the transformation of the distribution  $P(\text{Drug} \mid \text{molecule}, \text{target})$ , effectively addressing the data scarcity challenge identified earlier. More generation cases for CIDD are shown in Appendix E.

Utilizing this pairwise data enables fine-tuning of existing 3D-SBDD models, enhancing their ability to generate molecules that are both chemically plausible and meet multi-objective criteria for valid drugs. Unlike naive methods that modify a “good” molecule to create a “bad” version with a random distribution, our approach ensures that the distribution of “bad” molecules aligns closely with the output distribution of 3D-SBDD models. This alignment makes the data more compatible with existing frameworks, representing a significant contribution from a data-centric perspective.



**Figure 6. The CIDD framework generates molecules with both exceptional potency and favorable drug-like properties.** While 3D-SBDD models can produce molecules with strong 3D complementarity to target structures, these outputs often lack drug-like characteristics and are chemically unreasonable. In contrast, LLMs excel at generating chemically reasonable small molecules with good drug-likeness. CIDD effectively integrates the strengths of both approaches. Furthermore, the significant gap—or misalignment—between raw supporting molecules and widely accessible molecules was identified and quantified using novel metrics introduced in this work.

## 5. Research Rationale and Contribution Highlights

### 5.1. Problem Identification

In exploring how AI models could be applied to various stages of the drug discovery process, it is often the case that AI applications are directly copied from the key steps of the traditional drug development workflow without a thorough analysis of the content and meaning of the tasks. However, effectively applying AI in pharmaceutical science requires a focus on the core issues AI needs to solve, as well as an analysis of the new challenges and problems that arise as AI addresses these tasks.

Through research into the outputs of various 3D-SBDD models, we find that these outputs differ significantly from the traditional starting point of the “hit-to-lead” process. Specifically, the drug-likeness of these outputs is problematic, and the more challenging issue lies in the fact that many of these molecules are not even reasonable. Therefore, the problem faced by current 3D-SBDD models is not simply optimizing drug-likeness in the traditional “hit-to-lead” sense, but rather addressing the broader challenge of transforming unreasonable molecules into reasonable and drug-like candidates.

We believe that only by fully describing and demonstrating the gap between 3D-SBDD model results and compound structures widely accepted by (medicinal) chemists can we effectively bridge it, ultimately delivering practical benefits to AIDD and guiding its development in the right direction. In this work, by defining “MRR” and “AUR”, we effectively automate the identification of errors in model outputs regarding reasonability, specifically distinguishing unreasonable 3D-SBDD model outputs from molecules approved by (medicinal) chemists. Moreover, these two novel metrics are simple, relying solely on molecular topology, and do not depend on 3D conformation prediction or molecular property prediction. This is an important contribution, as it concretely highlights the misalignment between AI model outputs and molecules that can be broadly accepted and applied in pharmaceutical research. Furthermore, our algorithms can quantitatively measure this reasonability gap.

### 5.2. Problem Solving

Drug discovery aims to identify therapeutic molecules that satisfy all criteria for safety, efficacy, and controllable quality, including at least two dimensions: potency and drug-likeness. Potency is primarily influenced by the degree of 3D complementarity between designed small molecules and their intended target structures, while drug-likeness is

determined by the general physicochemical or biological properties of the small molecules. Potency is often roughly evaluated using docking scores, such as the Vina score, while metrics such as QED and SA are used to estimate drug-likeness. In this paper, we argue that a molecule must at least be “reasonable” to be considered drug-like, and drug-likeness can, in turn, be broken down into simple empirical rules, individual physicochemical metrics, and biological metrics (see Appendix B, C and D). We have successfully ensured that all detailed aspects of drug-likeness requirements are simultaneously and intelligently addressed within our framework.

In practical medicinal chemistry, the “hit-to-lead” process follows a problem-solving strategy, where each issue is addressed individually. It is a resource- and time-intensive process, often resulting in a trade-off between improving drug-likeness and decreasing potency, and vice versa. Therefore, this paper achieves a significant and challenging task: achieving substantial improvements in drug-likeness while maintaining potency.

Moreover, as previously discussed, challenges related to drug-likeness manifest in diverse ways depending on the specific characteristics of the molecule. For instance, certain compounds may exhibit inadequate water solubility, whereas others might face limitations in oral bio-availability. These variations underscore the necessity of tailoring strategies to enhance drug-likeness to the unique properties of each small molecule. Achieving this level of customization demands a thorough evaluation of multiple factors to develop the most effective optimization strategy—a process that traditionally requires extensive expertise, experience, and iterative experimentation by medicinal chemists. In this study, however, we have revolutionized this approach by harnessing the integrated knowledge and reasoning capabilities of LLMs to automate the process, marking a significant advancement in the field.

## 6. Conclusion and Future Works

In this paper, we introduced the **CIDD** framework, which addresses key limitations of traditional SBDD by integrating advanced 3D-SBDD models—capable of capturing molecular interactions—with LLMs, which excel in understanding drug-likeness requirements. Our evaluations on the Cross-Docked2020 dataset show that **CIDD** outperforms SOTA methods, achieving a higher success ratio defined by interaction ability and drug-likeness. This work pioneers the collaboration between domain-specific models and LLMs, demonstrating its effectiveness in molecular generation. Beyond this, **CIDD** can extend to other critical drug discovery stages, including **target identification**, **hit-to-lead optimization**, **preclinical toxicity evaluation**, and **synthetic pathway planning**, which we identify as future works. We

believe the collaboration between task-specific machine learning models and LLMs can revolutionize drug discovery, enabling a more efficient, interpretable, and impactful pipeline.

## References

- Achiam, J., Adler, S., Agarwal, S., Ahmad, L., Akkaya, I., Aleman, F. L., Almeida, D., Altenschmidt, J., Altman, S., Anadkat, S., et al. Gpt-4 technical report. *arXiv preprint arXiv:2303.08774*, 2023.
- Ahn, J., Verma, R., Lou, R., Liu, D., Zhang, R., and Yin, W. Large language models for mathematical reasoning: Progresses and challenges. *arXiv preprint arXiv:2402.00157*, 2024.
- Bickerton, G. R., Paolini, G. V., Besnard, J., Muresan, S., and Hopkins, A. L. Quantifying the chemical beauty of drugs. *Nature chemistry*, 4(2):90–98, 2012.
- Chakraborty, C., Bhattacharya, M., and Lee, S.-S. Artificial intelligence enabled chatgpt and large language models in drug target discovery, drug discovery, and development. *Molecular Therapy-Nucleic Acids*, 33:866–868, 2023.
- DeepSeek-AI, Liu, A., Feng, B., Xue, B., Wang, B., Wu, B., Lu, C., Zhao, C., Deng, C., Zhang, C., Ruan, C., Dai, D., Guo, D., Yang, D., Chen, D., Ji, D., Li, E., Lin, F., Dai, F., Luo, F., Hao, G., Chen, G., Li, G., Zhang, H., Bao, H., Xu, H., Wang, H., Zhang, H., Ding, H., Xin, H., Gao, H., Li, H., Qu, H., Cai, J. L., Liang, J., Guo, J., Ni, J., Li, J., Wang, J., Chen, J., Chen, J., Yuan, J., Qiu, J., Li, J., Song, J., Dong, K., Hu, K., Gao, K., Guan, K., Huang, K., Yu, K., Wang, L., Zhang, L., Xu, L., Xia, L., Zhao, L., Wang, L., Zhang, L., Li, M., Wang, M., Zhang, M., Zhang, M., Tang, M., Li, M., Tian, N., Huang, P., Wang, P., Zhang, P., Wang, Q., Zhu, Q., Chen, Q., Du, Q., Chen, R. J., Jin, R. L., Ge, R., Zhang, R., Pan, R., Wang, R., Xu, R., Zhang, R., Chen, R., Li, S. S., Lu, S., Zhou, S., Chen, S., Wu, S., Ye, S., Ye, S., Ma, S., Wang, S., Zhou, S., Yu, S., Zhou, S., Pan, S., Wang, T., Yun, T., Pei, T., Sun, T., Xiao, W. L., Zeng, W., Zhao, W., An, W., Liu, W., Liang, W., Gao, W., Yu, W., Zhang, W., Li, X. Q., Jin, X., Wang, X., Bi, X., Liu, X., Wang, X., Shen, X., Chen, X., Zhang, X., Chen, X., Nie, X., Sun, X., Wang, X., Cheng, X., Liu, X., Xie, X., Liu, X., Yu, X., Song, X., Shan, X., Zhou, X., Yang, X., Li, X., Su, X., Lin, X., Li, Y. K., Wang, Y. Q., Wei, Y. X., Zhu, Y. X., Zhang, Y., Xu, Y., Xu, Y., Huang, Y., Li, Y., Zhao, Y., Sun, Y., Li, Y., Wang, Y., Yu, Y., Zheng, Y., Zhang, Y., Shi, Y., Xiong, Y., He, Y., Tang, Y., Piao, Y., Wang, Y., Tan, Y., Ma, Y., Liu, Y., Guo, Y., Wu, Y., Ou, Y., Zhu, Y., Wang, Y., Gong, Y., Zou, Y., He, Y., Zha, Y., Xiong, Y., Ma, Y., Yan, Y., Luo, Y., You, Y., Liu, Y., Zhou, Y., Wu, Z. F., Ren, Z. Z., Ren, Z., Sha, Z., Fu, Z., Xu, Z., Huang, Z.,

- Zhang, Z., Xie, Z., Zhang, Z., Hao, Z., Gou, Z., Ma, Z., Yan, Z., Shao, Z., Xu, Z., Wu, Z., Zhang, Z., Li, Z., Gu, Z., Zhu, Z., Liu, Z., Li, Z., Xie, Z., Song, Z., Gao, Z., and Pan, Z. Deepseek-v3 technical report, 2024. URL <https://arxiv.org/abs/2412.19437>.
- Degen, J., Wegscheid-Gerlach, C., Zaliani, A., and Rarey, M. On the art of compiling and using 'drug-like' chemical fragment spaces. *ChemMedChem*, 3(10):1503, 2008.
- Ertl, P. and Schuffenhauer, A. Estimation of synthetic accessibility score of drug-like molecules based on molecular complexity and fragment contributions. *Journal of cheminformatics*, 1:1–11, 2009.
- Francoeur, P. G., Masuda, T., Sunseri, J., Jia, A., Iovanisci, R. B., Snyder, I., and Koes, D. R. Three-dimensional convolutional neural networks and a cross-docked data set for structure-based drug design. *Journal of chemical information and modeling*, 60(9):4200–4215, 2020.
- GLM, T., Zeng, A., Xu, B., Wang, B., Zhang, C., Yin, D., Zhang, D., Rojas, D., Feng, G., Zhao, H., et al. Chatglm: A family of large language models from glm-130b to glm-4 all tools. *arXiv preprint arXiv:2406.12793*, 2024.
- Guan, J., Qian, W. W., Peng, X., Su, Y., Peng, J., and Ma, J. 3d equivariant diffusion for target-aware molecule generation and affinity prediction. *arXiv preprint arXiv:2303.03543*, 2023.
- Guan, J., Zhou, X., Yang, Y., Bao, Y., Peng, J., Ma, J., Liu, Q., Wang, L., and Gu, Q. Decomppdiff: diffusion models with decomposed priors for structure-based drug design. *arXiv preprint arXiv:2403.07902*, 2024.
- Guo, D., Yang, D., Zhang, H., Song, J., Zhang, R., Xu, R., Zhu, Q., Ma, S., Wang, P., Bi, X., et al. Deepseek-r1: Incentivizing reasoning capability in llms via reinforcement learning. *arXiv preprint arXiv:2501.12948*, 2025.
- Hong, S., Zheng, X., Chen, J., Cheng, Y., Wang, J., Zhang, C., Wang, Z., Yau, S. K. S., Lin, Z., Zhou, L., et al. Metagpt: Meta programming for multi-agent collaborative framework. *arXiv preprint arXiv:2308.00352*, 2023.
- Ioakimidis, L., Thoukydidis, L., Mirza, A., Naeem, S., and Reynisson, J. Benchmarking the reliability of qikprop. correlation between experimental and predicted values. *QSAR & Combinatorial Science*, 27(4):445–456, 2008.
- Liévin, V., Hother, C. E., Motzfeldt, A. G., and Winther, O. Can large language models reason about medical questions? *Patterns*, 5(3), 2024.
- Liu, A., Feng, B., Wang, B., Wang, B., Liu, B., Zhao, C., Dengr, C., Ruan, C., Dai, D., Guo, D., et al. Deepseek-v2: A strong, economical, and efficient mixture-of-experts language model. *arXiv preprint arXiv:2405.04434*, 2024.
- Long, S., Zhou, Y., Dai, X., and Zhou, H. Zero-shot 3d drug design by sketching and generating. *Advances in Neural Information Processing Systems*, 35:23894–23907, 2022.
- Luo, S., Guan, J., Ma, J., and Peng, J. A 3d generative model for structure-based drug design. *Advances in Neural Information Processing Systems*, 34:6229–6239, 2021.
- Peng, X., Luo, S., Guan, J., Xie, Q., Peng, J., and Ma, J. Pocket2mol: Efficient molecular sampling based on 3d protein pockets. In *International Conference on Machine Learning*, pp. 17644–17655. PMLR, 2022.
- Qu, Y., Qiu, K., Song, Y., Gong, J., Han, J., Zheng, M., Zhou, H., and Ma, W.-Y. Molcraft: Structure-based drug design in continuous parameter space. *arXiv preprint arXiv:2404.12141*, 2024.
- Rogers, D. and Hahn, M. Extended-connectivity fingerprints. *Journal of chemical information and modeling*, 50(5):742–754, 2010.
- Salentin, S., Schreiber, S., Haupt, V. J., Adasme, M. F., and Schroeder, M. Plip: fully automated protein–ligand interaction profiler. *Nucleic acids research*, 43(W1):W443–W447, 2015.
- Touvron, H., Lavril, T., Izacard, G., Martinet, X., Lachaux, M.-A., Lacroix, T., Rozière, B., Goyal, N., Hambro, E., Azhar, F., et al. Llama: Open and efficient foundation language models. *arXiv preprint arXiv:2302.13971*, 2023.
- Trott, O. and Olson, A. J. Autodock vina: improving the speed and accuracy of docking with a new scoring function, efficient optimization, and multithreading. *Journal of computational chemistry*, 31(2):455–461, 2010.
- Valentini, G., Malchiodi, D., Gliozzo, J., Mesiti, M., Soto-Gomez, M., Cabri, A., Reese, J., Casiraghi, E., and Robinson, P. N. The promises of large language models for protein design and modeling. *Frontiers in Bioengineering*, 3:1304099, 2023.

## A. Detailed Prompts and Responses for LEDD

In this section, we present the detailed workflow of the CIDD framework, including the prompts and example responses for each module.

Figure 7 illustrates the complete drug design pipeline. The Interaction Module first identifies key fragments within the supporting molecule that interact with the protein pocket. This information is then utilized by the Design Module, which devises strategies to replace uncommon or unfavorable fragments while preserving crucial interactions. Once a new molecule is designed, the Evaluation Phase within the Design Module assesses its viability. Finally, the Reflection Module analyzes the design process and outcomes, highlighting both strengths and areas for improvement.

Figure 8 presents the prompt and example response for the Interaction Analysis Module.

Figures 9 and 10 display the prompt and example response for the Design Module.

Figures 11, 12, and 13 illustrate the prompt and example responses for the Reflection Module.

Figures 14 and 15 show the prompt and example response for the Selection Module.

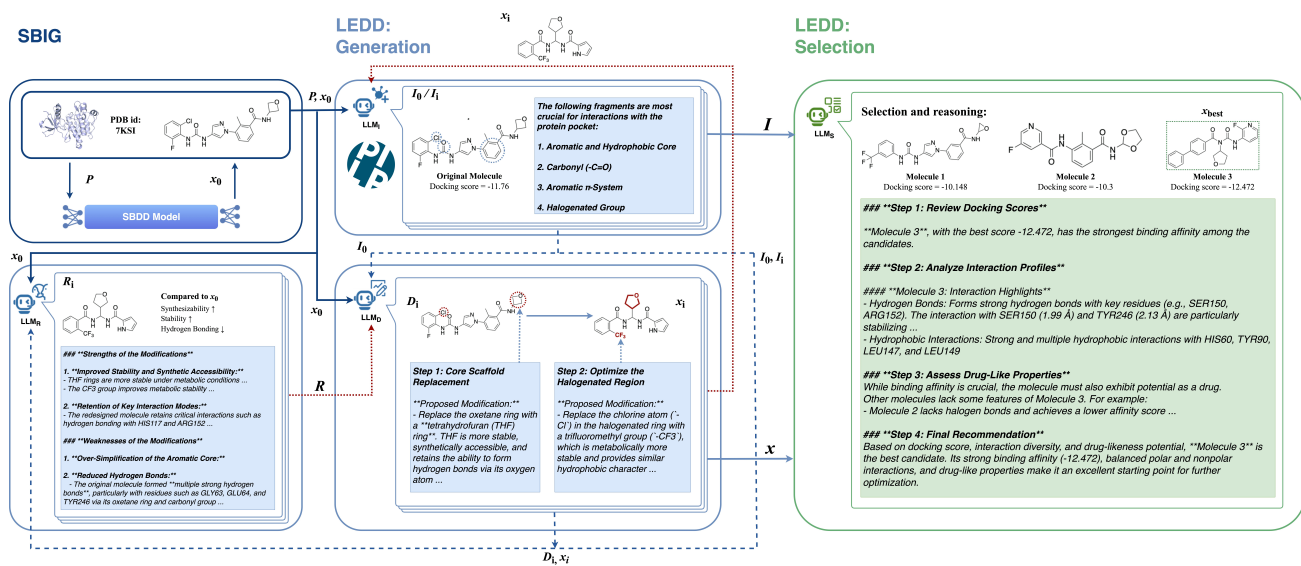


Figure 7. Workflow of CIDD framework

## Interaction analysis

The interaction analysis results are as follows: **[PLIP(Docking( $x_0, P$ ))]**  
 The smiles string of the molecule is: **[ $x_0$ ]**

**[Important]** Using the information from the interaction analysis and the fragment labels, based on the coordinates matching, you need to identify the key fragment on the molecule that conduct the interaction with the protein pocket.  
**[Important]** The format should be, which fragment can interact with which residue in the protein pocket. For example: The fragment 'ethanol' can interact with the residue 'ASP123' in the protein pocket.  
**[Important]** It should be at fragment level, instead of atom level. You need use the information from the fragment labels to identify which atom belongs to which fragment.



Query



LLM<sub>I</sub>

**Output [ $I_0$ ]:**

### \*\*Key Fragments of Importance\*\*  
 Based on the analysis, the following fragments are most crucial for interactions with the protein pocket:

1. \*\*Aromatic and Hydrophobic Core:\*\*  
  - [C]C1=C[C]=C[C]=C1` (Atoms: 5-11)  
 - Critical for hydrophobic interactions with ILE113, LEU142, and LEU147. This fragment anchors the molecule in the hydrophobic pocket.
2. \*\*Carbonyl (-C=O):\*\*  
  - Atoms '12, 13'  
 - Vital for hydrogen bonds, particularly with GLY63 and GLU64. This fragment contributes to the specificity of the interaction.
3. \*\*Oxetane Ring:\*\*  
  - [C]1[C][C]O1` (Atoms: 15-18)  
 - Key for hydrogen bonding with TYR246, providing excellent specificity and strength.
4. \*\*Aromatic π-System:\*\*  
  - [C]1=NN[C]=C1` (Atoms: 0-4)  
 - Engaged in π-stacking with TYR90, stabilizing the ligand in the binding pocket.
5. \*\*Halogenated Group:\*\*  
  - 'FC1=CC(Cl)=C[C]=C1` (Atoms: 23-30)  
 - Responsible for halogen bonding with PHE61, contributing to unique and specific interactions.

Figure 8. Interaction analysis module

## Design - Part 1

### [Instruction]

This is the original molecule:  $[x_0]$

This is the interaction analysis:  $[I_0]$

Based on the interaction analysis, design modifications to the original molecule. Your job is scaffold hopping: change the core scaffold structure while retaining key pharmacophores.

### [Design Objectives]

1. The modified molecule should be more stable and easier to synthesize than the original molecule. The new fragments should be common, stable and not weird.
2. The modified molecule should retain key properties of the original molecule, such as shape, size, and functionality.
3. The modified molecule should contain the key interaction types with the same residues as the original molecule.
4. The original molecule may contain uncommon or unstable fragments. Identify these fragments and replace them with more common and stable counterparts, ensuring that the modifications retain key properties of the original molecule, such as shape, size, and functionality. For instance, you might replace cyclohexadiene with benzene.
5. The modified molecule should be more like a drug candidate than the original molecule.

### [Design Requirements]

1. Do not modify the molecule too much.
2. Please only give the modification steps, do not generate smiles by yourself. We will use another agent to generate the new molecule based on your design.

### [Experience Summary]

We have done some modifications before. You can learn from the previous designs and reflections to make better modifications.

Here is the summary of the previous designs and reflections:  $[R]$

Now, give us the modification suggestions and requirements.



### Output $[D_1]$ :

#### ### \*\*Step 1: Core Scaffold Replacement\*\*

##### \*\*Unstable or Uncommon Scaffold:\*\*

- The original scaffold contains an oxetane ring ([C]1[C][C]O1), which, while beneficial for solubility and hydrogen bonding, can be chemically unstable under metabolic conditions and is synthetically challenging.

##### \*\*Proposed Modification:\*\*

- Replace the oxetane ring with a \*\*tetrahydrofuran (THF) ring\*\*. THF is more stable, synthetically accessible, and retains the ability to form hydrogen bonds via its oxygen atom. Importantly, it maintains a similar size, shape, and polarity.

#### ### \*\*Step 2: Optimize the Halogenated Region\*\*

##### \*\*Uncommon or Unstable Fragment:\*\*

- The halogenated aromatic fragment (FC1=CC(Cl)=C[C]=C1) can contribute to metabolic instability or toxicity (especially with chlorine) in some cases. The position and type of halogenation also determine interaction strength.

##### \*\*Proposed Modification:\*\*

- Replace the chlorine atom ('-Cl') in the halogenated ring with a trifluoromethyl group ('-CF<sub>3</sub>'), which is metabolically more stable and provides similar hydrophobic character and electronic properties to maintain halogen-bonding interactions. The fluorine atom can remain unaltered.

#### ### \*\*Step 3: Revise the Aromatic Core\*\*

##### \*\*Uncommon or Unstable Fragment:\*\*

- The core ring [C]C1=C[C]=[C][C]=C1 is a polycyclic conjugated system prone to oxidative metabolism. While it provides hydrophobicity and anchors the molecule, replacing it with a more common aromatic fragment (e.g., phenyl) can reduce metabolic liabilities without compromising interactions.

##### \*\*Proposed Modification:\*\*

- Replace [C]C1=C[C]=[C][C]=C1 with \*\*a phenyl ring (benzene)\*\*. Phenyl rings retain hydrophobicity and size while reducing the likelihood of oxidation and increasing synthetic accessibility.

Figure 9. Design Module

## Design - Part 2


**Output  $[D_1]$ :**

**### Step 4: Replace the 1,2,4-Triazine Ring\*\***  
**\*\*Uncommon or Unstable Fragment:\*\***  
- The '[C]1=NN[C]=C1' (1,2,4-triazine ring) involved in  $\pi$ -stacking with TYR90 can be retained, but this structure is not very common in drug-like scaffolds and may pose synthetic challenges.

**\*\*Proposed Modification:\*\***  
- Replace the 1,2,4-triazine ring with a \*\*pyridine ring (C5H5N)\*\*. Pyridine maintains aromaticity and hydrogen bond acceptor potential (via the nitrogen atom) for  $\pi$ -stacking but is more drug-like and easier to synthesize.

**### Step 5: Simplify Linker Chains\*\***  
**\*\*Uncommon or Unstable Fragment:\*\***  
- The linker fragment connecting the oxetane ring and other parts of the molecule may introduce unnecessary flexibility, which can lead to entropic penalties upon binding.

**\*\*Proposed Modification:\*\***  
- Shorten the linker chain by removing or simplifying alkyl groups. Use fewer methylene groups where applicable to reduce flexibility while maintaining shape and size for proper binding.

**### Summary of Modifications\*\***

1. \*\*Oxetane Ring (Unstable/Uncommon):\*\* Replace with \*\*THF ring\*\* to improve stability and synthetic accessibility while retaining hydrogen-bonding capability.
2. \*\*Halogenated Aromatic Ring (Metabolic Liability):\*\* Replace chlorine ('Cl') with \*\*trifluoromethyl group ('CF3')\*\* to improve metabolic stability while maintaining hydrophobic interactions and halogen bonding.
3. \*\*Polycyclic Aromatic Core (Oxidative Risk):\*\* Replace '[C]C1=C[C]=[C][C]=C1' with a \*\*phenyl ring (benzene)\*\* to reduce metabolic liability while retaining hydrophobicity.
4. \*\*1,2,4-Triazine Ring (Uncommon Scaffold):\*\* Replace with a \*\*pyridine ring\*\* to retain  $\pi$ -stacking and hydrogen-bond acceptor potential while improving drug-likeness.
5. \*\*Flexible Linkers (Entropic Penalty):\*\* Simplify and rigidify linker regions by shortening alkyl chains, reducing flexibility.

This is the original molecule:  $[x_0]$ 
**This is the modification designed by the design expert:  $[D_1]$** 
 **Query**

Change the molecule structure based on the modification designed by the design expert. Importantly, the modified molecule should be valid and make sense in the context of medicinal chemistry.

Now please only return the smiles string of the generated molecule. The smiles string should be enclosed in a pair of \$\$. For example: \$\$cccc\$\$\$


**Output  $[x_1]$ :**

```
$$$$C1=CC(C(F)(F)F)=C(C(=O)NC(C2CCOC2)NC(=O)C3=CC=CN3)C=C1$$$$
```

Figure 10. Design Module

## Reflection - Part 1

**[Instruction]**

This is the original molecule structure:  $[x_0]$

This is the interaction analysis of this molecule and the protein pocket:  $[I_0]$

This is the modification design generated by you:  $[D_1]$

This is the molecule structure designed based on your modification:  $[x_1]$

This is the interaction analysis generated by interaction export agent:  $[I_1]$

Previously, we asked you to modify a molecule to get a new molecule that binds better to the protein pocket. We analyzed the binding of the new molecule to the protein pocket and put it together with the binding before the modification for comparison.

Based on these analyses, you need to reflect on the previous modification and provide feedback on the design. Besides, we hope you can find out which fragments inside the structure of these two molecules are useful for binding to the protein pocket.

Please use critical thinking to analyze, pointing out both the good and the bad points. Your reflection is:



Query



LLMR

**Output  $[R_1]$ :****### Strengths of the Modifications\*\*****1. \*\*Improved Stability and Synthetic Accessibility:\*\***

- Replacing the \*\*oxetane ring\*\* with a \*\*tetrahydrofuran (THF) ring\*\* is a commendable adjustment. THF rings are more stable under metabolic conditions, while retaining key hydrogen-bonding interactions and similar steric bulk.

This was a sensible change that aligns well with drug-likeness principles.

- Removing the \*\*chlorine atom\*\* in favor of a \*\*trifluoromethyl (CF3) group\*\* was another thoughtful modification. The CF3 group improves metabolic stability and reduces potential toxicity from reactive halogens, while maintaining the original hydrophobicity and shape.

**2. \*\*Retention of Key Interaction Modes:\*\***

- The redesigned molecule retains critical interactions such as hydrogen bonding with HIS117 and ARG152, hydrophobic interactions with HIS60, LEU147, and PHE188, and  $\pi$ -stacking with TYR90. These interactions are crucial for binding affinity and ensure the molecule continues to engage the protein pocket effectively.

- The \*\*pyridine ring\*\* (replacing the less common 1,2,4-triazine ring) aligns better with drug-likeness rules while maintaining hydrogen bonding and hydrophobic capabilities. This substitution strengthens the molecule's pharmacokinetic prospects.

**3. \*\*Refinement of Scaffolds and Simplification:\*\***

- Simplifying the polycyclic aromatic core into a \*\*benzene ring\*\* was a reasonable modification to reduce oxidation-prone elements. This ensures the molecule is more stable and synthetically tractable without losing significant hydrophobic interactions.

**### Weaknesses of the Modifications\*\*****1. \*\*Reduction in Docking Score:\*\***

- The docking score decreased from \*\*-11.76 (original molecule)\*\* to \*\*-9.215 (modified molecule)\*\*, indicating a clear drop in binding affinity. While the modified molecule retains key interactions, some critical binding contributions were inadvertently weakened during redesign. The TEF reduction suggests a loss of key complementary contacts between the ligand and protein pocket.

**2. \*\*Over-Simplification of the Aromatic Core:\*\***

- Replacing the conjugated aromatic system (' $[C]C1=C[C]=[C][C]=C1$ ') with a simple \*\*benzene ring\*\* reduced the hydrophobic surface area and  $\pi$ -electron system available for interactions. Consequently, hydrophobic interactions with residues like TYR90, ILE113, and LEU142 were diminished, and the molecule lost some of its ability to stabilize key  $\pi$ -interactions within the pocket.

**3. \*\*Unutilized Potential of the Trifluoromethyl Group:\*\***

- While the trifluoromethyl (CF3) group improved metabolic stability, it did not directly contribute to binding interactions within the protein pocket. This functional group occupies space but does not engage with any specific residues, effectively adding to molecular weight without enhancing binding. A better-placed or functionally active replacement could have yielded greater interaction strength.

## Reflection - Part 2


LLM<sub>R</sub>

**Output [R<sub>1</sub>]:**

4. \*\*Reduced Hydrogen Bonds:\*\*  
 - The original molecule formed \*\*multiple strong hydrogen bonds\*\*, particularly with residues such as GLY63, GLU64, and TYR246 via its oxetane ring and carbonyl group. These hydrogen bonds were either weakened or lost in the redesign, with new hydrogen bonds (forming with HIS117 and ARG152) failing to fully compensate for this depletion.

5. \*\*Flexibility in the THF Ring:\*\*  
 - While the THF ring is more stable than the oxetane ring, it likely introduces greater flexibility due to its *sp*<sup>3</sup>-hybridized carbons. This flexibility may lead to entropic penalties upon binding, making the molecule less efficient in achieving a preorganized, bioactive conformation.

6. \*\*Over-Reliance on Hydrophobic Interactions:\*\*  
 - Similar to the original molecule, the modified structure still relies heavily on \*\*hydrophobic interactions\*\* for binding (e.g., HIS60, TYR90, LEU147). Hydrophobic interactions are less specific than polar or ionic interactions, which are critical for selectivity and affinity. By not introducing additional polar groups, the redesign missed an opportunity to improve overall binding specificity.

#### \*\*Comparison of Binding Fragments\*\*

#### \*\*Original Molecule:\*\*

1. \*\*Oxetane Ring (Lost in the Redesign):\*\*  
 - Forms key hydrogen bonds with TYR246 in the binding pocket, contributing significantly to specific and strong ligand binding. Its removal weakened overall binding affinity.
2. \*\*Conjugated Hydrophobic Core ('[C]C1=C[C]=C[C]=C1'):\*\*  
 - Provides extensive hydrophobic and  $\pi$ -stacking interactions with residues such as ILE113, LEU142, and TYR90. Replacing this rich aromatic structure with a benzene ring reduced the hydrophobic and  $\pi$ -electron contribution to binding.
3. \*\*Halogenated Aromatic Ring ('FC1=CC(Cl)=C[C]=C1'):\*\*  
 - Engages the protein via halogen bonding with PHE61, adding specificity to binding interactions. Replacing chlorine with CF<sub>3</sub> abolished some halogen bonds, weakening protein-ligand complementarity.

#### \*\*Modified Molecule:\*\*

1. \*\*THF Ring (Introduced):\*\*  
 - Retains the ability to form hydrogen bonds (e.g., with ARG152). However, its introduction has caused greater flexibility and entropic penalties that may offset its stabilizing contributions.
2. \*\*Trifluoromethyl Group (CF<sub>3</sub>, Introduced):\*\*  
 - Metabolically stable and hydrophobic but does not directly interact with the protein. Its placement on the aromatic ring adds molecular weight but no functional enhancement to binding.
3. \*\*Pyridine Ring (Introduced):\*\*  
 - Maintains hydrogen-bonding with HIS117 and interacts hydrophobically with HIS60, performing well as a replacement for 1,2,4-triazine. Though not as inherently diverse in interaction opportunities as its predecessor, it improves the drug-likeness of the molecule.
4. \*\*Benzene Ring (Simplified):\*\*  
 - While it retains some hydrophobic interaction capability, this fragment no longer engages residues like TYR90 or PHE188 as robustly as the original conjugated aromatic system. This reduced binding affinity.

Figure 12. Reflection Module

## Reflection - Part 3


Output [ $R_1$ ]:

**### \*\*Key Fragments Retained or Lost for Binding\*\***

\*\*Critical Retained Fragments:\*\*

1. \*\*Pyridine Ring\*\* for  $\pi$ -stacking and hydrogen bonding with TYR90 and HIS117.
2. \*\*Hydrogen Bonding Carbonyl Group\*\* interacting with HIS117 and ARG152.

\*\*Critical Fragments Lost:\*\*

1. \*\*Oxetane Ring\*\* contributed unusually strong hydrogen bonds to TYR246, which were lost in the redesign.
2. \*\*Conjugated Hydrophobic Core\*\* ensured multisite hydrophobic interactions and  $\pi$ -stacking with residues like LEU142 and TYR90.
3. \*\*Halogenated Aromatic Ring\*\* provided halogen bonds with PHE61, contributing unique specificity lost in the redesign.

**### \*\*Suggestions for Improvement\*\***

1. \*\*Reintroduce Hydrogen Bonding Groups:\*\*  
- Add back polar fragments (e.g., hydroxyl, amide groups) to increase hydrogen-bonding capacity with residues like TYR246, GLY63, and GLU64.
2. \*\*Revisit the Aromatic Core:\*\*  
- Instead of oversimplifying the hydrophobic core to benzene, consider a polycyclic aromatic or heterocyclic system to balance hydrophobicity and metabolic stability.
3. \*\*Optimize Trifluoromethyl Group Placement:\*\*  
- Move or replace the CF<sub>3</sub> group with a fragment that directly engages residues in the protein pocket (e.g., a difluorophenyl or hydrophilic substituent).
4. \*\*Rigidify the THF Ring:\*\*  
- Lock the THF ring into a constrained system (e.g., fused bicyclic rings) to reduce flexibility and entropic penalties.

**### \*\*Conclusion\*\***

The modifications resulted in a molecule that is synthetically and metabolically improved but less effective in binding to the protein pocket, as indicated by the diminished docking score. While retaining important interactions, the redesign lost too many advantageous fragments (e.g., oxetane, conjugated aromatic core). Future optimizations should aim to restore lost interactions, improve hydrogen bonding, and balance hydrophobicity with polar contacts for stronger and more specific binding.

Figure 13. Reflection Module

## Selection - Part 1

**[Instruction]**

Given a protein pocket and a number of different molecules, I need you to find a molecule that is best suited to bind this protein pocket. We will provide you with interaction reports for each molecule and protein pocket and ask you to make choices based on this information. You should consider both the binding analysis and whether the molecule has potential to be a real drug. You should output the reason and the smiles string of the chosen molecule. The smiles string should be enclosed in a pair of \$\$. For example: ...*(The reason)* The chosen smiles is: \$\$CCO\$\$.

This is the molecule structure:  $[x_n]$   
 This is the interaction analysis of this molecule and the protein pocket:  $[I_n]$

---

This is the molecule structure:  $[x_m]$   
 This is the interaction analysis of this molecule and the protein pocket:  $[I_m]$

---

This is the molecule structure:  $[x_p]$   
 This is the interaction analysis of this molecule and the protein pocket:  $[I_p]$

---

Please think step by step:


  
Query



**The chosen molecule is:**  
 $O=C(C1=CC=C(C=C1)C2=CC=CC=C2)N(C3CCOC3)C(NC4=C(F)N=CC=C4)=O$   
 The docking score of the chosen molecule is: -12.472  
 The reason for choosing the molecule is: To select the best molecule for binding to the protein pocket, we will step through the following considerations:

**### \*\*Step 1: Review Docking Scores\*\***  
 The docking score is a key metric indicating the binding affinity between a molecule and the protein pocket. Lower docking scores (more negative values) suggest stronger binding. The docking scores for the respective molecules are as follows:  
 1. Molecule 1: -10.148  
 2. Molecule 2: -10.3  
 3. Molecule 3: -12.472

From this, \*\*Molecule 3\*\*, with the best score of \*\*-12.472\*\*, has the strongest binding affinity among the candidates.

**### \*\*Step 2: Analyze Interaction Profiles\*\***  
 Building off the docking scores, we now consider the rich interaction profiles of each molecule. A molecule that forms diverse interactions will often bind more robustly and specifically to the protein pocket.

**#### \*\*Molecule 3: Interaction Highlights\*\***

- **Hydrophobic Interactions:** Strong and multiple hydrophobic interactions with HIS60, TYR90, LEU147, and LEU149, anchored by the aromatic benzene ring.
- **Hydrogen Bonds:** Forms strong hydrogen bonds with key residues (e.g., SER150, ARG152). The interaction with SER150 (1.99 Å) and TYR246 (2.13 Å) are particularly stabilizing.
- **π-Stacking:** Strong π-stacking with TYR90 (T-shaped geometry).
- **π-Cation Interactions:** Robust π-cation interaction with ARG152 (3.85 Å), stabilized further by ideal offset alignment (1.32 Å).
- **Halogen Bonds:** Two halogen bonds with GLU189 (3.84 Å) and ASN237 (3.40 Å) provide an additional layer of interaction, making this molecule unique in its interaction diversity.

Figure 14. Selection Module

## Selection - Part 2



LLMs

**\*\*Key Strengths:\*\***

- The interaction diversity and strength of Molecule 3 far surpass other molecules, leveraging hydrophobic forces, hydrogen bonding,  $\pi$ -stacking,  $\pi$ -cation interactions, and halogen bonding.
- The molecule effectively anchors itself to both polar and nonpolar regions, ensuring specificity for the protein pocket.

**### \*\*Step 3: Assess Drug-Like Properties\*\***

While binding affinity is crucial, the molecule must also exhibit potential as a drug.

Properties relevant to drug-likeness include:

- **Hydrophobic Components:** Ensure solubility and stability for membrane diffusion.
- **Hydrogen Bonding Groups:** Contribute to specificity and bioactivity.
- **Halogen Incorporation:** Enhances membrane permeability and metabolic stability.
- **Compact, Non-Bulky Structure:** Ensures the molecule fits within the protein pocket without steric clashes.

For Molecule 3:

- The combination of aromatic rings, amide groups, and fluorine atoms supports balanced hydrophobic and polar properties, increasing stability and bioavailability.
- The inclusion of halogens enhances drug-likeness further.

Other molecules lack some features of Molecule 3. For example:

- Molecule 2 lacks halogen bonds and achieves a lower affinity score.
- Molecule 1 have good binding but lack the breadth of interactions seen with Molecule 3.

**### \*\*Step 4: Final Recommendation\*\***

Based on docking score, interaction diversity, and drug-likeness potential, **Molecule 3** is the best candidate. Its strong binding affinity (-12.472), balanced polar and nonpolar interactions, and drug-like properties make it an excellent starting point for further optimization.

**### \*\*Chosen Molecule\*\***

**Reason:** Molecule 3 exhibits the highest docking score, with diverse interaction types (hydrophobic, hydrogen bonding,  $\pi$ -stacking,  $\pi$ -cation, and halogen bonding) that secure it in critical regions of the protein pocket. Additionally, it offers promising drug-like features such as halogen incorporation and a well-optimized molecular structure.

**Selected SMILES String:**

\$\$\$\$O=C(C1=CC=C(C=C1)C2=CC=CC=C2)N(C3CCOC3)C(NC4=C(F)N=CC=C4)=O\$\$\$\$

Figure 15. Selection Module

## B. Algorithm for MRR and AUR

The complete calculation process for assessing the reasonability of a molecule is outlined in Algorithm 1.

**Algorithm 1** Evaluation of Molecular Reasonability**Input:** Molecule object (*mol*)**Output:** Molecular Reasonability (*MRR*) and Atom Unreasonable Ratio (*AUR*)**Step 1: Detect Carbonyl and Imine Group Carbons**Initialize an empty list for *carbonyl/imine carbons*.**foreach** *bond* in *mol* **do****if** *bond* is double and one atom is carbon, the other is oxygen or nitrogen **then**  
    Record the carbon atom in *carbonyl/imine groups*.**Step 2: Identification of Ring Systems**Identify all ring structures and their corresponding atom indices within *mol*.

Calculate the number of atoms in each ring.

**foreach** *ring* in the molecule **do****if** the ring shares one or more atoms with another ring **then**  
    Group the connected rings into a single *ring system*.**Step 3: Evaluation of Molecular Reasonability**

Exclude any atoms previously identified as part of carbonyl or imine groups.

Classify the remaining carbon atoms in each ring system as follows:

- *sp*<sup>2</sup> hybridized: Aromatic or unsaturated carbons.

- Non-*sp*<sup>2</sup> hybridized: Saturated carbons.

**foreach** *ring system* in the *ring systems* **do****if** the *ring system* contains multiple rings and all carbon atoms are non-*sp*<sup>2</sup> **then**  
    Mark the molecule as unreasonable.  
    Add the atoms to the unreasonable atom list.**foreach** *ring system* in the remaining *ring systems* **do****foreach** *ring* in the *ring system* **do**  
**if** all carbon atoms within the *ring* are consistent in hybridization (either all *sp*<sup>2</sup> or all non-*sp*<sup>2</sup>) **then**  
    Mark the *ring* as reasonable.  
**else**  
    Add the *ring* to the remaining *ring list*.**while** the remaining *ring list* is not empty **do****foreach** *ring* in the remaining *ring list* **do**  
    Exclude atoms that have already been classified as reasonable.  
**if** all remaining carbon atoms are consistent in hybridization (either all *sp*<sup>2</sup> or all non-*sp*<sup>2</sup>) **then**  
    Mark the *ring* as reasonable.  
**if** no new reasonable rings are identified **then**  
    Mark the molecule as unreasonable.  
    Add the carbon atoms in the remaining rings to the unreasonable atom list.  
    **Exit the loop.**Calculate *AUR* as the ratio of unreasonable atom count to the total ring atom count.**Return** *MRR* and *AUR*.

## C. QikProp properties

The full set of properties used for the QikProp pass ratio analysis is presented in Table 4.

The QikProp filter applied in the main text incorporates a comprehensive range of criteria provided by QikProp, including "#stars", "#amine", "#amidine", "#acid", "#amide", "#rotor", "#rtvFG", "mol\_MW", "dipole", "SASA", "FOSA", "FISA", "PISA", "WPSA", "volume", "donorHB", "acceptHB", "dip<sup>2</sup>/V", "ACxDN·5/SA", "glob", "QPolarz", "QPllogPC16", "QPllogPoct", "QPllogPw", "QPllogPo/w", "QPllogS", "CIQPllogS", "QPPCaco", "QPllogBB", "QPPMDCK", "QPllogKp", "IP(eV)", "EA(eV)", "#metab", "QPllogKhsa", "PercentHumanOralAbsorption", "SAFluorine", "SAAmideO", "PSA", "#Nando", and "RuleOfThree".

Table 4. QikProp Properties and Descriptors

Property or Descriptor	Description	Range or Recommended Values
Molecule name	The molecule's identifier derived from the title line in the input structure file. If no title is provided, the file name is used.	
#stars	Count of descriptors or properties falling outside the 95% range for known drugs. A higher count indicates reduced drug-likeness.	0 – 5
#amine	Total non-conjugated amine groups present in the molecule.	0 – 1
#amidine	Number of amidine or guanidine functional groups in the structure.	0
#acid	Quantity of carboxylic acid groups in the molecule.	0 – 1
#amide	Count of non-conjugated amide groups.	0 – 1
#rotor	Number of rotatable bonds that are neither trivial nor sterically hindered.	0 – 15
#rtvFG	Total reactive functional groups present in the molecule, potentially affecting stability or toxicity.	0 – 2
mol_MW	Molecular weight of the compound.	130.0 – 725.0
Dipole	Calculated dipole moment of the molecule in Debye units.	1.0 – 12.5
SASA	Solvent-accessible surface area (SASA) in square angstroms, measured with a probe of 1.4 Å radius.	300.0 – 1000.0
FOSA	Hydrophobic part of the SASA, representing saturated carbon and attached hydrogen atoms.	0.0 – 750.0
FISA	Hydrophilic fraction of the SASA, encompassing polar atoms like nitrogen and oxygen.	7.0 – 330.0
PISA	SASA component attributable to π-systems.	0.0 – 450.0
WPSA	Weakly polar component of the SASA, including atoms like halogens, phosphorus, and sulfur.	0.0 – 175.0
Volume	Total solvent-accessible volume in cubic angstroms, determined with a 1.4 Å radius probe.	500.0 – 2000.0
donorHB	Estimated number of hydrogen bonds donated to water in solution.	0.0 – 6.0
acceptHB	Estimated number of hydrogen bonds accepted from water.	2.0 – 20.0
Dip <sup>2</sup> /V	Dipole moment squared divided by molecular volume, a key factor in solvation energy.	0.0 – 0.13
ACxDN <sup>0.5</sup> /SA	Cohesive interaction index in solids based on molecular properties.	0.0 – 0.05
glob	Descriptor measuring how close the shape of a molecule is to a sphere.	0.75 – 0.95
QPPolrz	Predicted molecular polarizability in cubic angstroms.	13.0 – 70.0
QPlogPC16	Predicted partition coefficient between hexadecane and gas phases.	4.0 – 18.0
QPlogPoct	Predicted partition coefficient between octanol and gas phases.	8.0 – 35.0
QPlogPw	Predicted partition coefficient between water and gas phases.	4.0 – 45.0
QPlogPo/w	Predicted partition coefficient between octanol and water phases.	2.0 – 6.5
QPlogS	Predicted solubility of the molecule in water (log S, in mol/L).	-6.5 – 0.5
CIQPlogS	Conformation-independent prediction of water solubility (log S).	-6.5 – 0.5
QPPCaco	Predicted permeability through Caco-2 cells, in nm/s.	<25 poor, >500 great
QPlogBB	Predicted partition coefficient for brain/blood.	-3.0 – 1.2
QPPMDCK	Predicted permeability through MDCK cells, in nm/s.	<25 poor, >500 great
QPlogKp	Predicted skin permeability (log Kp).	-8.0 – -1.0
IP(eV)	Ionization potential calculated using PM3.	7.9 – 10.5
EA(eV)	Electron affinity calculated using PM3.	-0.9 – 1.7
#metab	Predicted number of possible metabolic reactions.	1 – 8
QPlogKhsa	Predicted binding affinity to human serum albumin.	-1.5 – 1.5
HumanOralAbsorption	Qualitative assessment of oral absorption: 1 (low), 2 (medium), or 3 (high).	
PercentHumanOralAbsorption	Quantitative prediction of oral absorption percentage.	>80% high, <25% poor
SAFluorine	Solvent-accessible fluorine surface area.	0.0 – 100.0
SAAmideO	Solvent-accessible surface area of amide oxygen atoms.	0.0 – 35.0
PSA	Polar surface area, calculated for nitrogen, oxygen, and carbonyl groups.	7.0 – 200.0
#NandO	Total count of nitrogen and oxygen atoms.	2 – 15
RuleOffive	Number of Lipinski's Rule of Five violations.	Max 4
RuleOffthree	Number of Jorgensen's Rule of Three violations.	Max 3
#ringatoms	Count of atoms within molecular rings.	
#in34	Number of atoms in 3- or 4-membered rings.	
#in56	Number of atoms in 5- or 6-membered rings.	
#noncon	Number of ring atoms unable to form conjugated aromatic systems.	
#nonHatr	Count of heavy (non-hydrogen) atoms in the structure.	
Jm	Predicted maximum transdermal transport rate ( $\mu\text{g cm}^{-2} \text{ hr}^{-1}$ ).	

## D. More Experiment Results

Based on the different criteria presented in Table 4, we provide additional pass ratio results in Table 5.

Filter 1 is identical to the QikProp filter used in the main text.

Filter 2 removes some non-essential properties and focuses on well-defined physicochemical properties, including "#rtvFG", "QPlogS", "QPlogPo/w", "mol\_MW", "dipole", "SASA", "FOSA", "FISA", "IP(eV)", "EA(eV)", "#metab", "PercentHumanOralAbsorption", and "PSA".

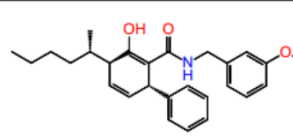
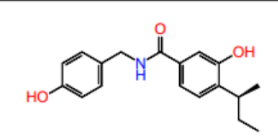
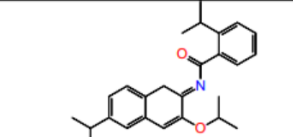
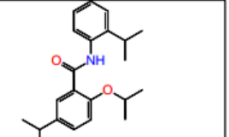
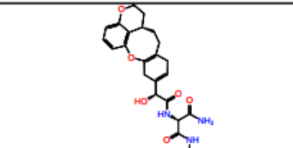
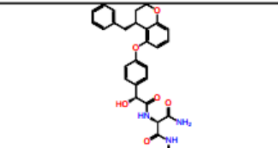
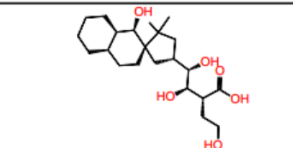
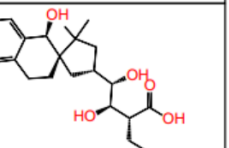
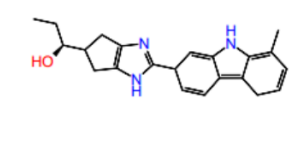
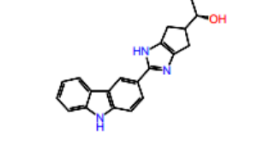
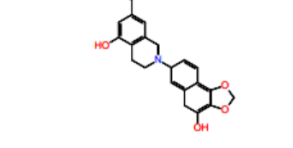
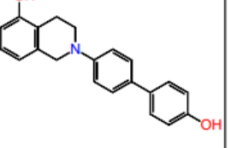
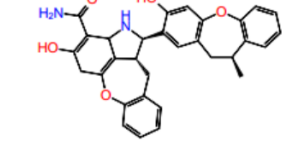
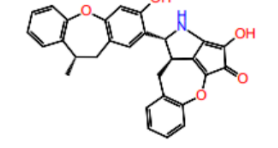
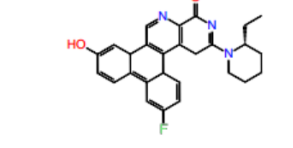
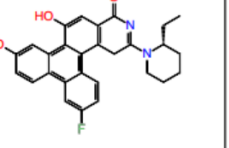
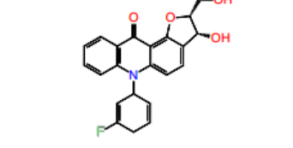
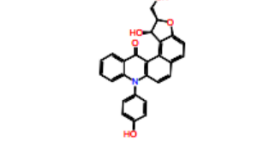
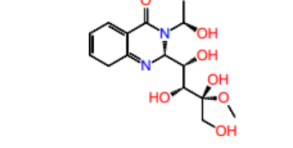
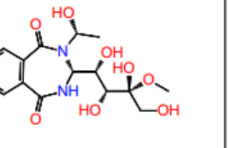
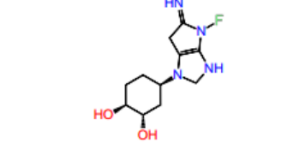
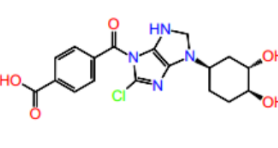
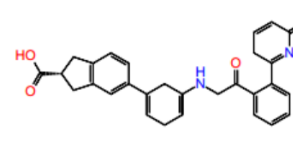
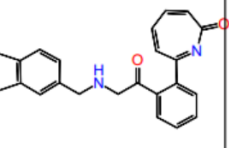
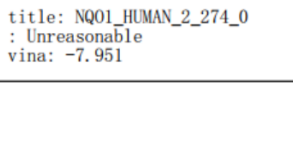
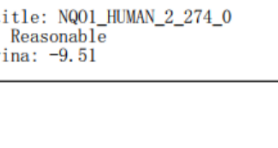
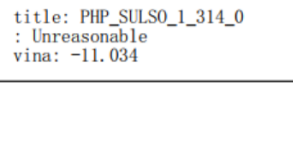
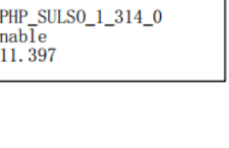
Filter 3 assesses molecular compliance with the "RuleOfFive" criterion. However, instead of allowing up to four violations as typically recommended, this filter adopts a stricter definition, considering only molecules that fully comply (i.e., setting the maximum allowable violations to zero).

*Table 5.* QikProp results for different methods with and without CIDD

Method	Filter 1	Filter 2	Filter 3
<b>Pocket2Mol</b>			
Original	29.58%	51.52%	89.58%
CIDD	56.97%	75.64%	92.24%
<b>TargetDiff</b>			
Original	26.32%	48.20%	69.47%
CIDD	53.37%	75.60%	81.85%
<b>DecompDiff</b>			
Original	29.04%	53.96%	55.14%
CIDD	37.54%	68.48%	65.64%
<b>MolCRAFT</b>			
Original	22.37%	43.52%	66.45%
CIDD	35.22%	63.23%	74.09%

## E. More cases

More generated molecules from CIDD are presented below. For each case, we display the initial supporting molecule derived from 3D-SBDD models alongside the final designed molecules produced by CIDD.

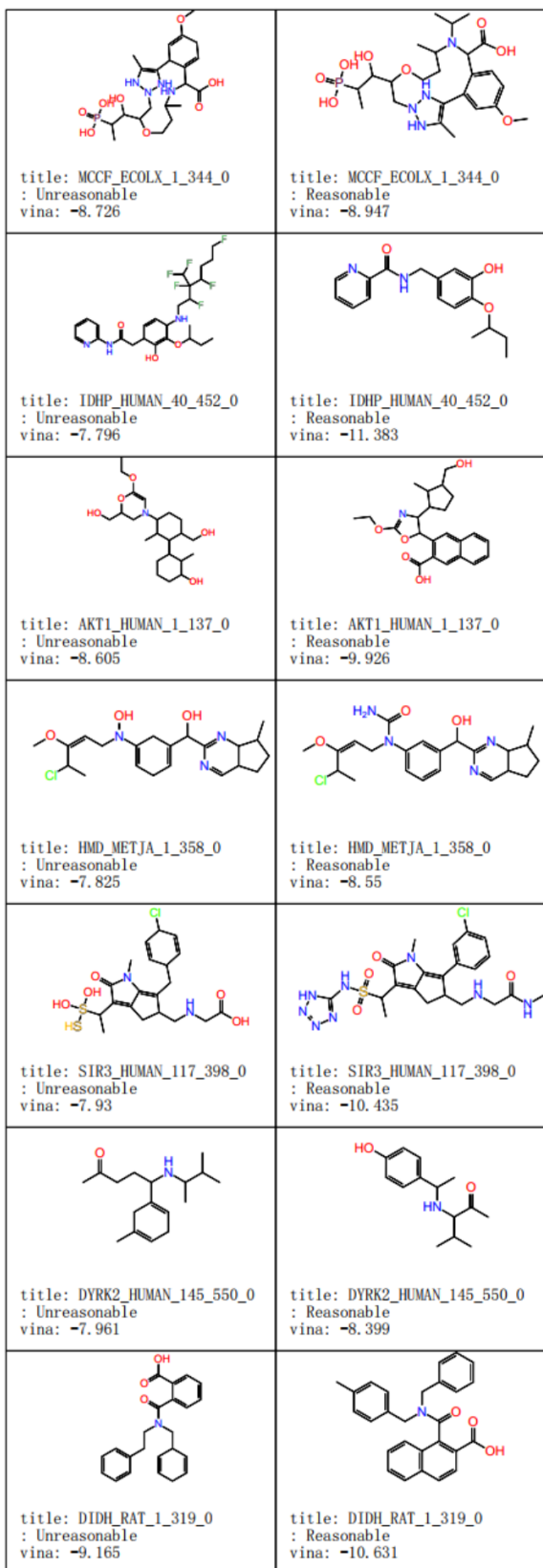
Supporting molecule	CIDD output	Supporting molecule	CIDD output
			
title: IDHP_HUMAN_40_452_0 : Unreasonable vina: -7.824	title: IDHP_HUMAN_40_452_0 : Reasonable vina: -10.106	title: IDHP_HUMAN_40_452_0 : Unreasonable vina: -7.941	title: IDHP_HUMAN_40_452_0 : Reasonable vina: -9.66
			
title: NOS1_HUMAN_302_723_0 : Unreasonable vina: -9.415	title: NOS1_HUMAN_302_723_0 : Reasonable vina: -10.098	title: NOS1_HUMAN_302_723_0 : Unreasonable vina: -8.054	title: NOS1_HUMAN_302_723_0 : Reasonable vina: -8.432
			
title: NOS1_HUMAN_302_723_0 : Unreasonable vina: -10.069	title: NOS1_HUMAN_302_723_0 : Reasonable vina: -10.22	title: NOS1_HUMAN_302_723_0 : Unreasonable vina: -9.287	title: NOS1_HUMAN_302_723_0 : Reasonable vina: -9.6
			
title: ABL2_HUMAN_274_551_0 : Unreasonable vina: -10.007	title: ABL2_HUMAN_274_551_0 : Reasonable vina: -10.946	title: ABL2_HUMAN_274_551_0 : Unreasonable vina: -9.916	title: ABL2_HUMAN_274_551_0 : Reasonable vina: -10.509
			
title: AK1BA_HUMAN_1_316_0 : Unreasonable vina: -10.421	title: AK1BA_HUMAN_1_316_0 : Reasonable vina: -10.778	title: AK1BA_HUMAN_1_316_0 : Unreasonable vina: -8.37	title: AK1BA_HUMAN_1_316_0 : Reasonable vina: -9.24
			
title: NQ01_HUMAN_2_274_0 : Unreasonable vina: -7.951	title: NQ01_HUMAN_2_274_0 : Reasonable vina: -9.51	title: NQ01_HUMAN_2_274_0 : Unreasonable vina: -8.37	title: NQ01_HUMAN_2_274_0 : Reasonable vina: -9.24
			
title: PHP_SULSO_1_314_0 : Unreasonable vina: -11.034	title: PHP_SULSO_1_314_0 : Reasonable vina: -11.397	title: PHP_SULSO_1_314_0 : Unreasonable vina: -11.034	title: PHP_SULSO_1_314_0 : Reasonable vina: -11.397

Supporting molecule	CIDD output	Supporting molecule	CIDD output
title: PHKG1_RABIT_6_296_ATPsite_0 : Unreasonable vina: -8.548	title: PHKG1_RABIT_6_296_ATPsite_0 : Reasonable vina: -8.727	title: BGL07_ORYSJ_25_504_0 : Unreasonable vina: -8.041	title: BGL07_ORYSJ_25_504_0 : Reasonable vina: -9.949
title: CD38_HUMAN_44_300_0 : Unreasonable vina: -7.443	title: CD38_HUMAN_44_300_0 : Reasonable vina: -8.863	title: TNKS2_HUMAN_948_1162_0 : Unreasonable vina: -10.284	title: TNKS2_HUMAN_948_1162_0 : Reasonable vina: -10.974
title: P2Y12_HUMAN_1_342_0 : Unreasonable vina: -10.463	title: P2Y12_HUMAN_1_342_0 : Reasonable vina: -10.674	title: HMD_METJA_1_358_0 : Unreasonable vina: -9.259	title: HMD_METJA_1_358_0 : Reasonable vina: -10.458
title: SQHC_ALIAD_1_631_0 : Unreasonable vina: -14.278	title: SQHC_ALIAD_1_631_0 : Reasonable vina: -17.408	title: SQHC_ALIAD_1_631_0 : Unreasonable vina: -13.626	title: SQHC_ALIAD_1_631_0 : Reasonable vina: -13.825
title: BGAT_HUMAN_63_353_0 : Unreasonable vina: -7.891	title: BGAT_HUMAN_63_353_0 : Reasonable vina: -9.201	title: CHIB_SERMA_1_499_0 : Unreasonable vina: -10.676	title: CHIB_SERMA_1_499_0 : Reasonable vina: -13.113
title: CHIB_SERMA_1_499_0 : Unreasonable vina: -7.115	title: CHIB_SERMA_1_499_0 : Reasonable vina: -8.719	title: NR1H4_HUMAN_258_486_0 : Unreasonable vina: -10.038	title: NR1H4_HUMAN_258_486_0 : Reasonable vina: -11.021

Supporting molecule	CIDD output	Supporting molecule	CIDD output
title: SDIA_ECOLI_1_171_0 : Unreasonable vina: -11.019	title: SDIA_ECOLI_1_171_0 : Reasonable vina: -11.294	title: SDIA_ECOLI_1_171_0 : Unreasonable vina: -8.52	title: SDIA_ECOLI_1_171_0 : Reasonable vina: -13.937
title: GSTP1_HUMAN_2_210_0 : Unreasonable vina: -7.591	title: GSTP1_HUMAN_2_210_0 : Reasonable vina: -8.725	title: HDHA_ECOLI_1_255_0 : Unreasonable vina: -7.709	title: HDHA_ECOLI_1_255_0 : Reasonable vina: -8.778
title: HDHA_ECOLI_1_255_0 : Unreasonable vina: -8.5	title: HDHA_ECOLI_1_255_0 : Reasonable vina: -8.515	title: NOS1_HUMAN_302_723_0 : Unreasonable vina: -11.943	title: NOS1_HUMAN_302_723_0 : Reasonable vina: -12.979
title: IDHP_HUMAN_40_452_0 : Unreasonable vina: -8.176	title: IDHP_HUMAN_40_452_0 : Reasonable vina: -10.774	title: NR1H4_HUMAN_258_486_0 : Unreasonable vina: -6.824	title: NR1H4_HUMAN_258_486_0 : Reasonable vina: -8.578
title: IDHP_HUMAN_40_452_0 : Unreasonable vina: -7.605	title: IDHP_HUMAN_40_452_0 : Reasonable vina: -11.661	title: CPXB_BACMB_2_464_0 : Unreasonable vina: -9.607	title: CPXB_BACMB_2_464_0 : Reasonable vina: -10.132
title: AK1BA_HUMAN_1_316_0 : Unreasonable vina: -9.845	title: AK1BA_HUMAN_1_316_0 : Reasonable vina: -9.981	title: P2Y12_HUMAN_1_342_0 : Unreasonable vina: -7.75	title: P2Y12_HUMAN_1_342_0 : Reasonable vina: -16.253
title: OLIAC_CANSA_1_101_0 : Unreasonable vina: -7.631	title: OLIAC_CANSA_1_101_0 : Reasonable vina: -8.866	title: SIR3_HUMAN_117_398_0 : Unreasonable vina: -8.238	title: SIR3_HUMAN_117_398_0 : Reasonable vina: -8.331

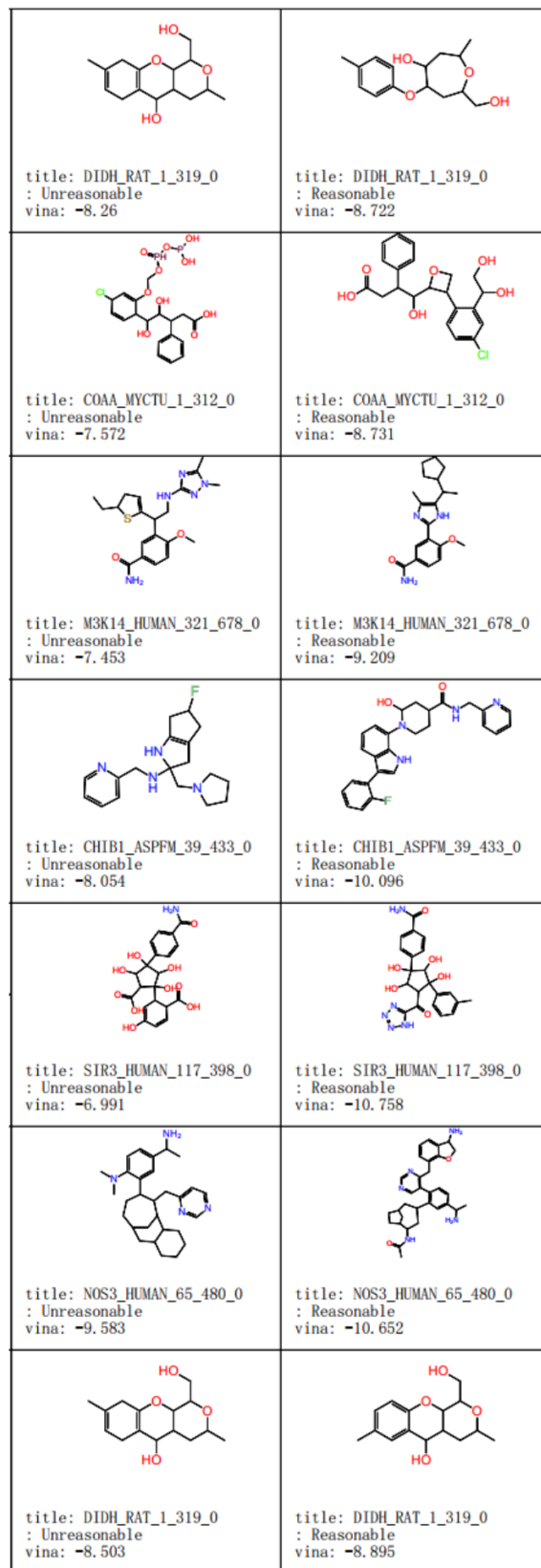
## Supporting molecule

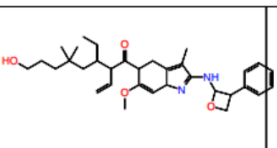
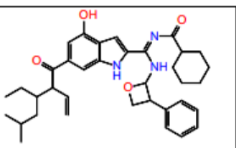
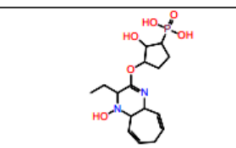
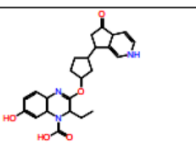
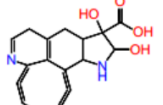
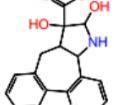
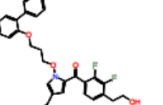
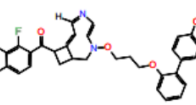
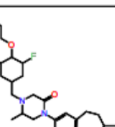
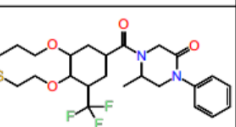
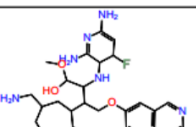
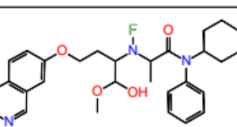
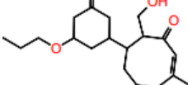
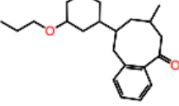
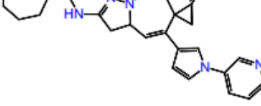
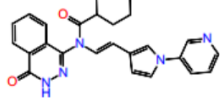
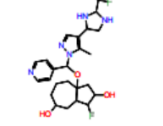
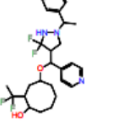
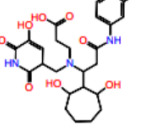
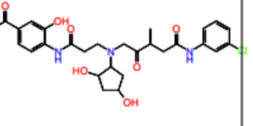
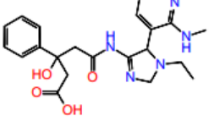
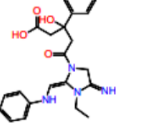
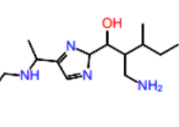
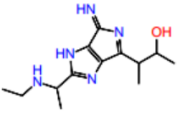
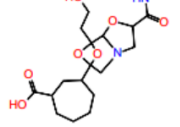
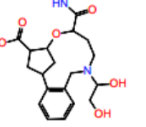
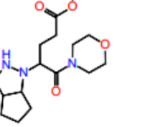
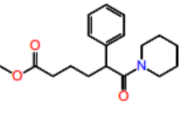
## CIDD output



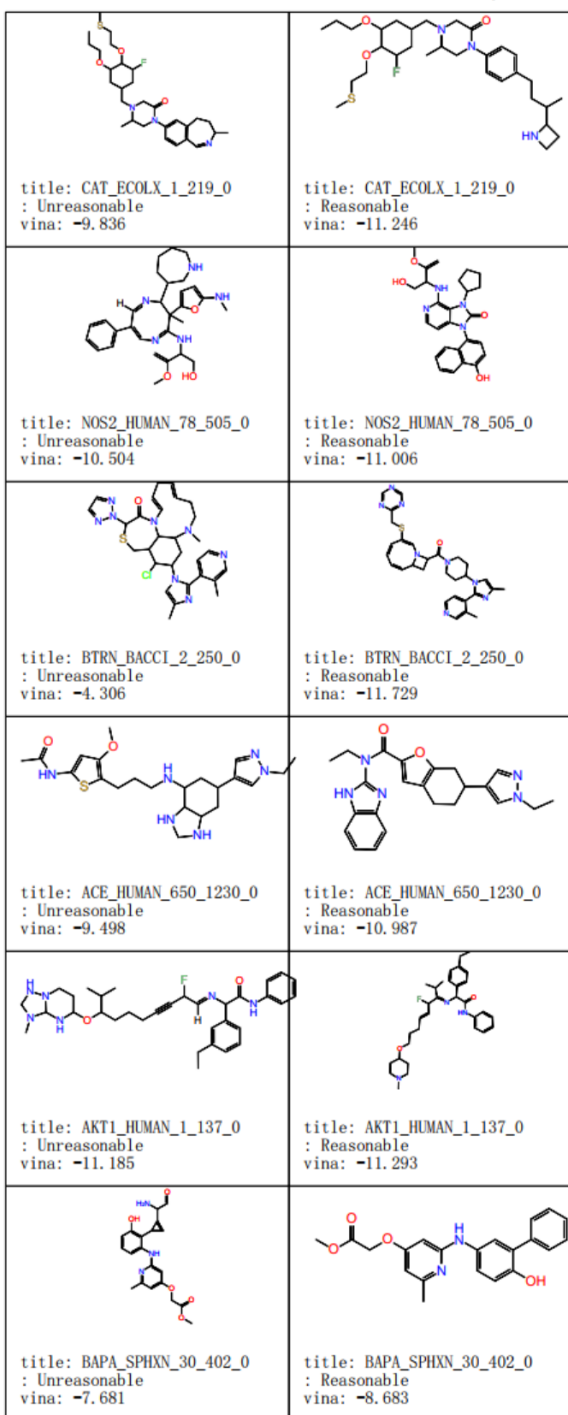
## Supporting molecule

## CIDD output



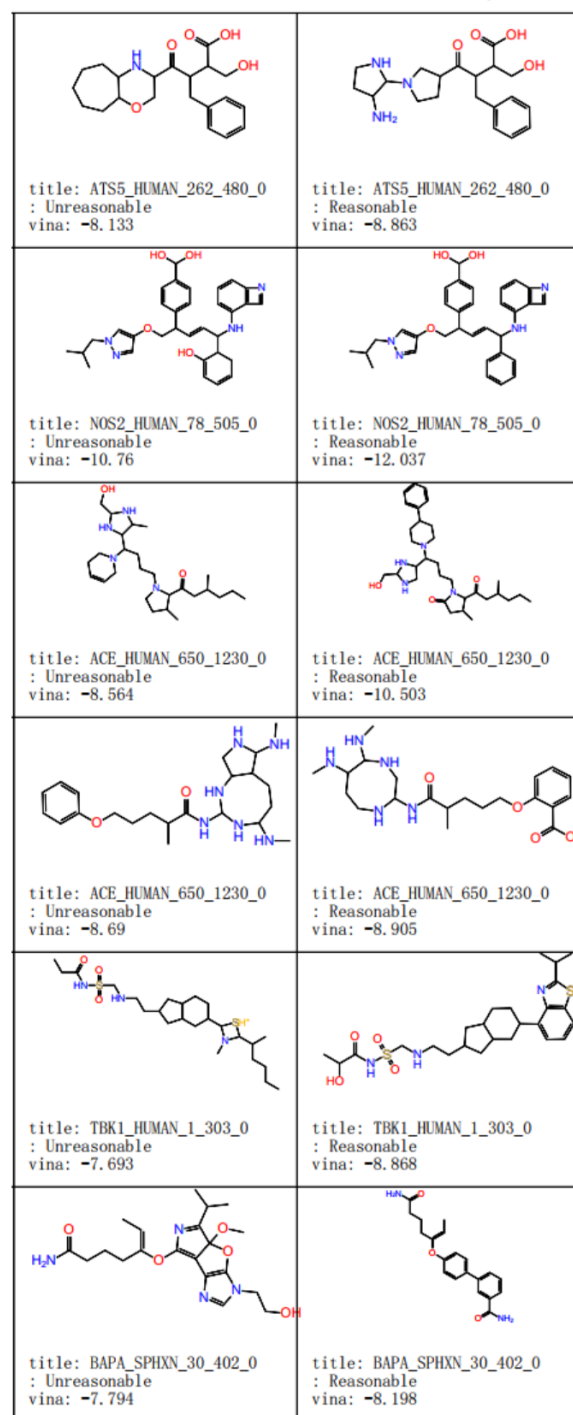
Supporting molecule	CIDD output	Supporting molecule	CIDD output
			
title: BACE2_HUMAN_76_460_0 : Unreasonable vina: -8.586	title: BACE2_HUMAN_76_460_0 : Reasonable vina: -9.854	title: GRK4_HUMAN_1_578_0 : Unreasonable vina: -7.158	title: GRK4_HUMAN_1_578_0 : Reasonable vina: -8.93
			
title: F16P1_HUMAN_1_338_0 : Unreasonable vina: -8.173	title: F16P1_HUMAN_1_338_0 : Reasonable vina: -8.633	title: CPXB_BACMB_2_464_0 : Unreasonable vina: -10.201	title: CPXB_BACMB_2_464_0 : Reasonable vina: -11.121
			
title: CAT_ECOLX_1_219_0 : Unreasonable vina: -9.838	title: CAT_ECOLX_1_219_0 : Reasonable vina: -10.164	title: BSD_ASPTE_1_130_0 : Unreasonable vina: -7.492	title: BSD_ASPTE_1_130_0 : Reasonable vina: -8.786
			
title: DFPA_LOLVU_2_314_0 : Unreasonable vina: -7.208	title: DFPA_LOLVU_2_314_0 : Reasonable vina: -8.581	title: RG1_RAUSE_1_513_0 : Unreasonable vina: -10.06	title: RG1_RAUSE_1_513_0 : Reasonable vina: -11.978
			
title: QPCT_HUMAN_33_361_0 : Unreasonable vina: -8.178	title: QPCT_HUMAN_33_361_0 : Reasonable vina: -9.527	title: QPCT_HUMAN_33_361_0 : Unreasonable vina: -7.531	title: QPCT_HUMAN_33_361_0 : Reasonable vina: -8.356
			
title: KS6A3_HUMAN_41_357_0 : Unreasonable vina: -8.242	title: KS6A3_HUMAN_41_357_0 : Reasonable vina: -8.738	title: GUX1_HYPJE_18_451_0 : Unreasonable vina: -7.25	title: GUX1_HYPJE_18_451_0 : Reasonable vina: -8.375
			
title: AROE_THET8_1_263_0 : Unreasonable vina: -8.741	title: AROE_THET8_1_263_0 : Reasonable vina: -8.794	title: UPPS_ECOLI_1_253_0 : Unreasonable vina: -7.288	title: UPPS_ECOLI_1_253_0 : Reasonable vina: -8.315

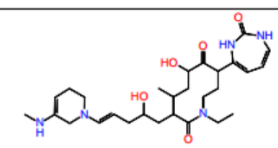
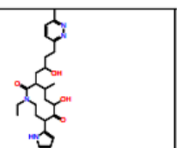
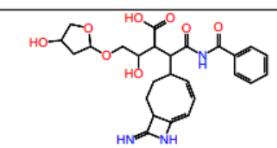
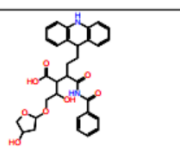
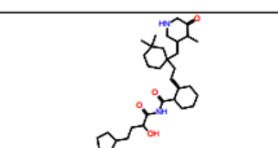
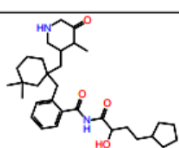
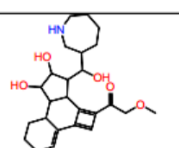
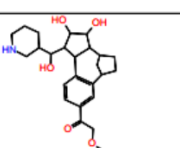
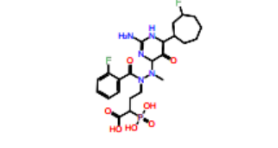
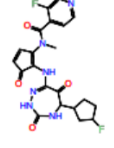
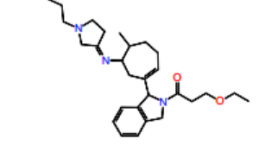
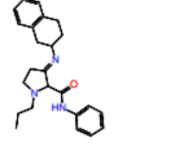
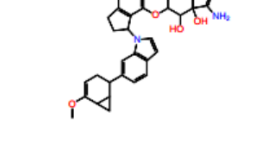
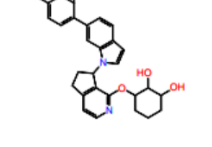
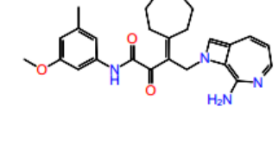
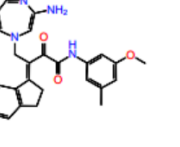
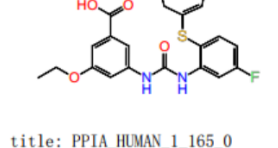
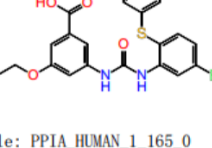
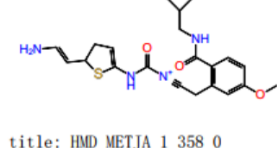
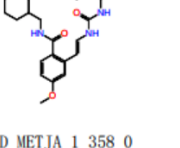
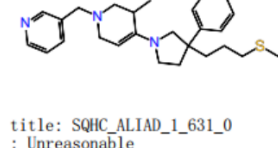
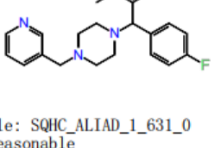
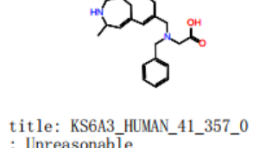
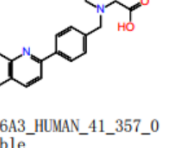
## Supporting molecule



## CIDD output

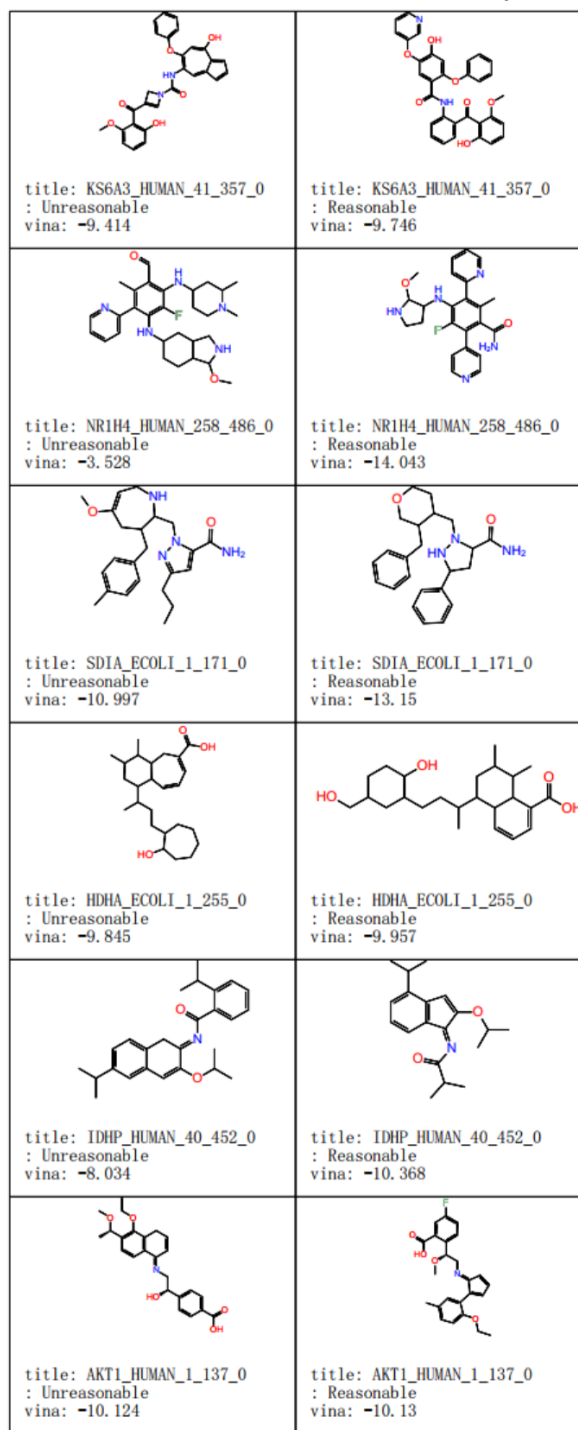
## Supporting molecule



Supporting molecule	CIDD output	Supporting molecule	CIDD output
			
title: PHKG1_RABIT_6_296_ATPsite_0 : Unreasonable vina: -8.922	title: PHKG1_RABIT_6_296_ATPsite_0 : Reasonable vina: -9.205	title: BGL07_ORYSJ_25_504_0 : Unreasonable vina: -10.446	title: BGL07_ORYSJ_25_504_0 : Reasonable vina: -10.592
			
title: RG1_RAUSE_1_513_0 : Unreasonable vina: -10.484	title: RG1_RAUSE_1_513_0 : Reasonable vina: -11.024	title: DPP2_HUMAN_27_492_0 : Unreasonable vina: -9.855	title: DPP2_HUMAN_27_492_0 : Reasonable vina: -11.224
			
title: CD38_HUMAN_44_300_0 : Unreasonable vina: -8.72	title: CD38_HUMAN_44_300_0 : Reasonable vina: -9.327	title: PTGIS_HUMAN_20_500_0 : Unreasonable vina: -8.318	title: PTGIS_HUMAN_20_500_0 : Reasonable vina: -9.448
			
title: XANLY_BACGL_26_777_0 : Unreasonable vina: -9.053	title: XANLY_BACGL_26_777_0 : Reasonable vina: -9.483	title: PPIA_HUMAN_1_165_0 : Unreasonable vina: -8.777	title: PPIA_HUMAN_1_165_0 : Reasonable vina: -10.083
			
title: PPIA_HUMAN_1_165_0 : Unreasonable vina: -8.023	title: PPIA_HUMAN_1_165_0 : Reasonable vina: -8.605	title: HMD_METJA_1_358_0 : Unreasonable vina: -8.349	title: HMD_METJA_1_358_0 : Reasonable vina: -9.593
			
title: SQHC_ALIAD_1_631_0 : Unreasonable vina: -11.51	title: SQHC_ALIAD_1_631_0 : Reasonable vina: -14.292	title: KS6A3_HUMAN_41_357_0 : Unreasonable vina: -8.967	title: KS6A3_HUMAN_41_357_0 : Reasonable vina: -11.101

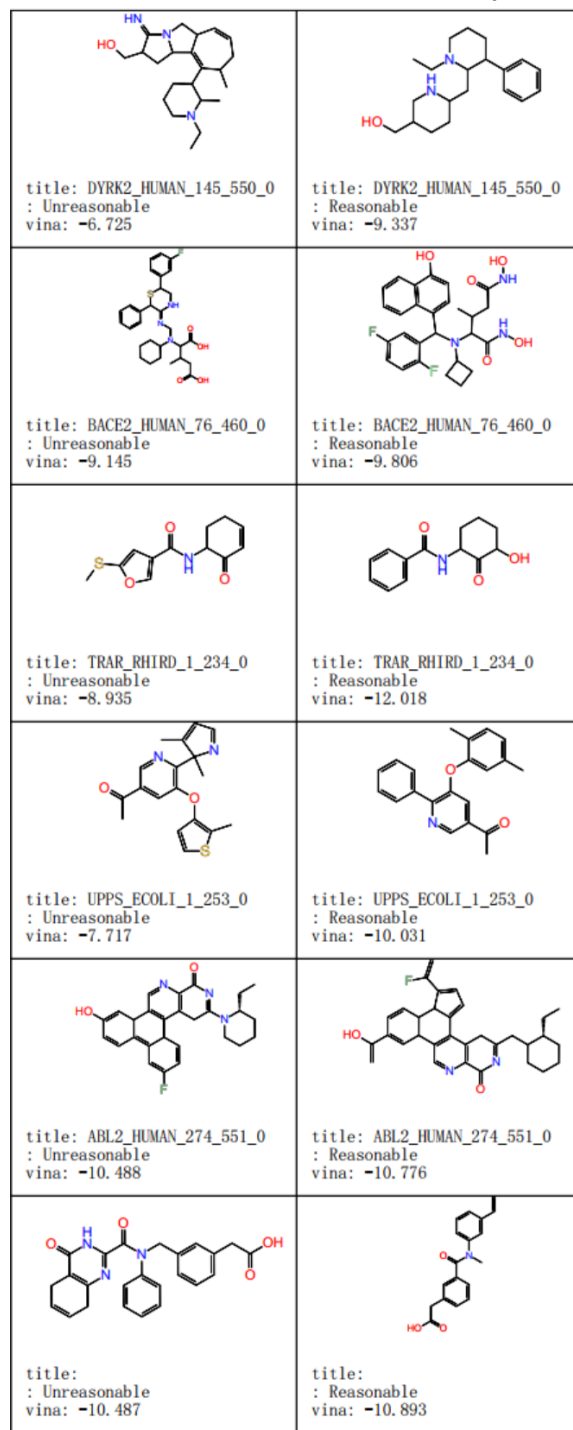
## Supporting molecule

## CIDD output



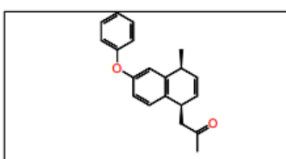
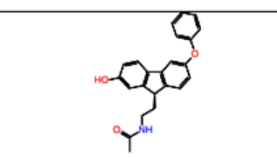
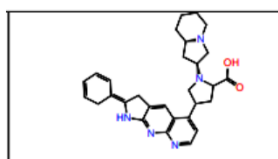
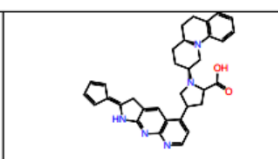
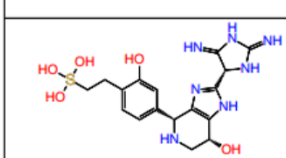
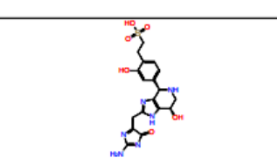
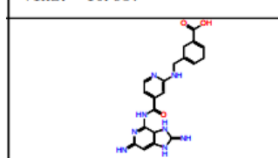
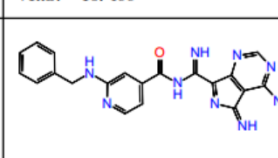
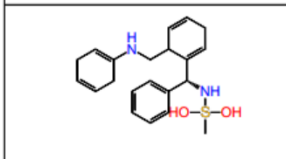
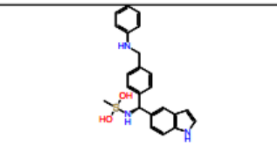
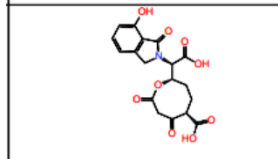
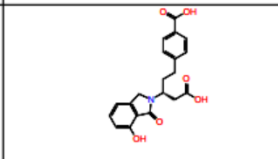
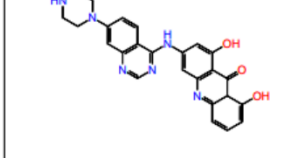
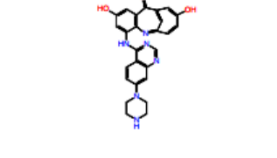
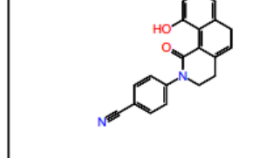
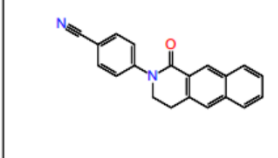
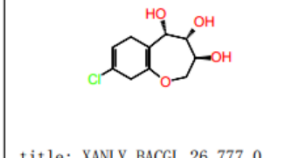
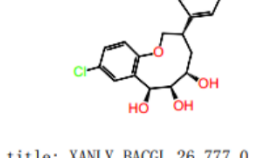
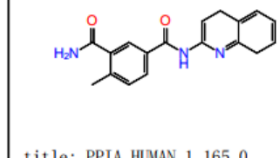
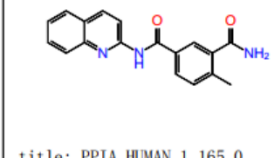
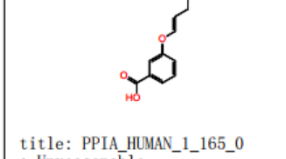
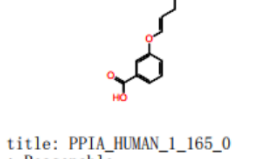
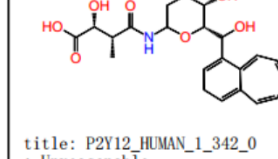
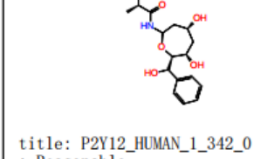
## Supporting molecule

## CIDD output



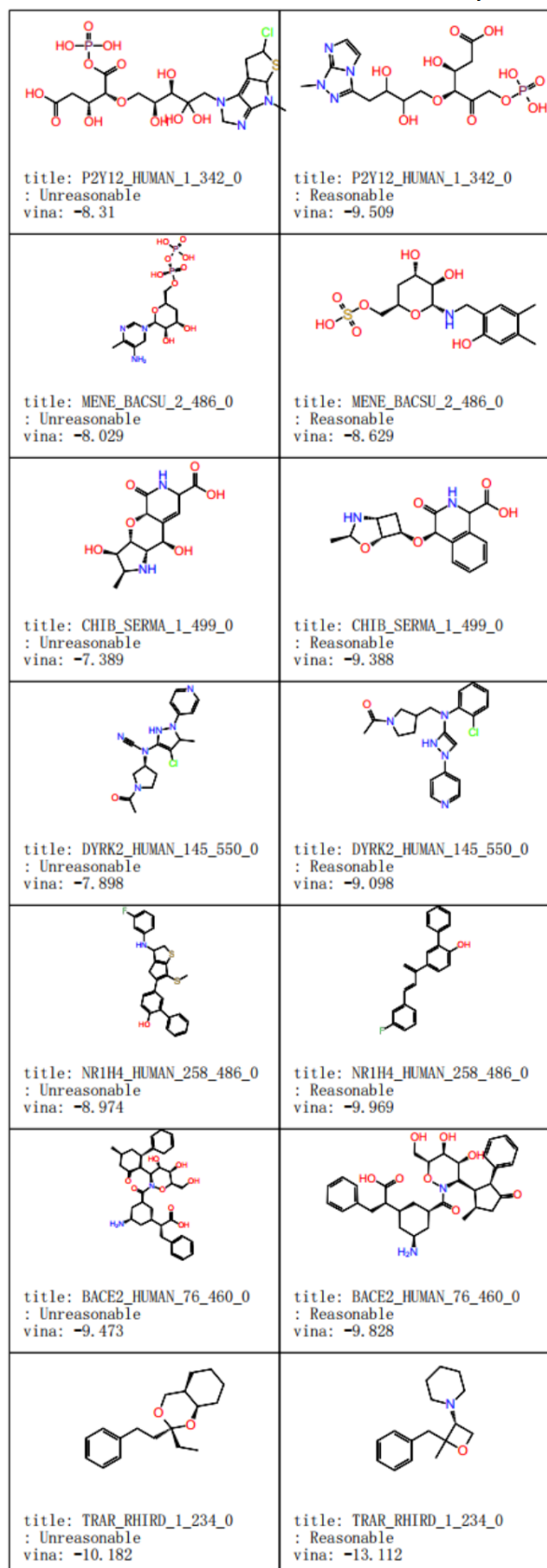
Supporting molecule	CIDD output	Supporting molecule	CIDD output
title: MURA_ECOLI_1_419_catalytic_0 : Unreasonable vina: -8.295	title: MURA_ECOLI_1_419_catalytic_0 : Reasonable vina: -9.241	title: BGL07_ORYSJ_25_504_0 : Unreasonable vina: -8.028	title: BGL07_ORYSJ_25_504_0 : Reasonable vina: -9.632
title: PAC_ECOLX_27_846_0 : Unreasonable vina: -9.538	title: PAC_ECOLX_27_846_0 : Reasonable vina: -10.042	title: P2Y12_HUMAN_1_342_0 : Unreasonable vina: -8.514	title: P2Y12_HUMAN_1_342_0 : Reasonable vina: -8.942
title: EXG1_CANAL_41_438_0 : Unreasonable vina: -9.965	title: EXG1_CANAL_41_438_0 : Reasonable vina: -10.569	title: FKB1A_HUMAN_2_108_0 : Unreasonable vina: -7.899	title: FKB1A_HUMAN_2_108_0 : Reasonable vina: -8.786
title: CHIB_SERMA_1_499_0 : Unreasonable vina: -9.972	title: CHIB_SERMA_1_499_0 : Reasonable vina: -10.354	title: KS6A3_HUMAN_41_357_0 : Unreasonable vina: -7.827	title: KS6A3_HUMAN_41_357_0 : Reasonable vina: -8.545
title: SDIA_ECOLI_1_171_0 : Unreasonable vina: -10.933	title: SDIA_ECOLI_1_171_0 : Reasonable vina: -11.339	title: GUX1_HYPJE_18_451_0 : Unreasonable vina: -10.767	title: GUX1_HYPJE_18_451_0 : Reasonable vina: -12.3

Supporting molecule	CIDD output	Supporting molecule	CIDD output
title: HDHA_ECOLI_1_255_0 : Unreasonable vina: -8.511	title: HDHA_ECOLI_1_255_0 : Reasonable vina: -9.995	title: ODBB_THET8_1_324_0 : Unreasonable vina: -9.002	title: ODBB_THET8_1_324_0 : Reasonable vina: -9.322
title: IDHP_HUMAN_40_452_0 : Unreasonable vina: -8.039	title: IDHP_HUMAN_40_452_0 : Reasonable vina: -9.819	title: CPXB_BACMB_2_464_0 : Unreasonable vina: -9.196	title: CPXB_BACMB_2_464_0 : Reasonable vina: -12.034
title: NOS1_HUMAN_302_723_0 : Unreasonable vina: -9.495	title: NOS1_HUMAN_302_723_0 : Reasonable vina: -9.579	title: NOS1_HUMAN_302_723_0 : Unreasonable vina: -10.062	title: NOS1_HUMAN_302_723_0 : Reasonable vina: -10.305
title: CAT_ECOLX_1_219_0 : Unreasonable vina: -9.2	title: CAT_ECOLX_1_219_0 : Reasonable vina: -13.057	title: BSD_ASPTE_1_130_0 : Unreasonable vina: -8.807	title: BSD_ASPTE_1_130_0 : Reasonable vina: -9.501
title: ABL2_HUMAN_274_551_0 : Unreasonable vina: -10.702	title: ABL2_HUMAN_274_551_0 : Reasonable vina: -11.583	title: NQO1_HUMAN_2_274_0 : Unreasonable vina: -9.262	title: NQO1_HUMAN_2_274_0 : Reasonable vina: -10.424
title: BTRN_BACCI_2_250_0 : Unreasonable vina: -8.786	title: BTRN_BACCI_2_250_0 : Reasonable vina: -8.951	title: NAGZ_VIBCH_1_330_0 : Unreasonable vina: -7.206	title: NAGZ_VIBCH_1_330_0 : Reasonable vina: -8.307
title: AKT1_HUMAN_1_137_0 : Unreasonable vina: -10.1	title: AKT1_HUMAN_1_137_0 : Reasonable vina: -11.478	title: AKT1_HUMAN_1_137_0 : Unreasonable vina: -12.405	title: AKT1_HUMAN_1_137_0 : Reasonable vina: -13.048

Supporting molecule	CIDD output	Supporting molecule	CIDD output
			
title: PA21B_PIG_23_146_0 : Unreasonable vina: -8.391	title: PA21B_PIG_23_146_0 : Reasonable vina: -10.029	title: PHKG1_RABIT_6_296_ATPSite_0 : Unreasonable vina: -10.937	title: PHKG1_RABIT_6_296_ATPSite_0 : Reasonable vina: -13.466
			
title: M3K14_HUMAN_321_678_0 : Unreasonable vina: -8.948	title: M3K14_HUMAN_321_678_0 : Reasonable vina: -9.001	title: M3K14_HUMAN_321_678_0 : Unreasonable vina: -9.44	title: M3K14_HUMAN_321_678_0 : Reasonable vina: -9.899
			
title: PTGIS_HUMAN_20_500_0 : Unreasonable vina: -7.955	title: PTGIS_HUMAN_20_500_0 : Reasonable vina: -9.193	title: PAC_ECOLX_27_846_0 : Unreasonable vina: -7.907	title: PAC_ECOLX_27_846_0 : Reasonable vina: -8.704
			
title: PAC_ECOLX_27_846_0 : Unreasonable vina: -9.272	title: PAC_ECOLX_27_846_0 : Reasonable vina: -9.421	title: TNKS2_HUMAN_948_1162_0 : Unreasonable vina: -10.215	title: TNKS2_HUMAN_948_1162_0 : Reasonable vina: -12.537
			
title: XANLY_BACGL_26_777_0 : Unreasonable vina: -6.991	title: XANLY_BACGL_26_777_0 : Reasonable vina: -8.994	title: PPIA_HUMAN_1_165_0 : Unreasonable vina: -9.243	title: PPIA_HUMAN_1_165_0 : Reasonable vina: -9.435
			
title: PPIA_HUMAN_1_165_0 : Unreasonable vina: -7.765	title: PPIA_HUMAN_1_165_0 : Reasonable vina: -8.447	title: P2Y12_HUMAN_1_342_0 : Unreasonable vina: -8.744	title: P2Y12_HUMAN_1_342_0 : Reasonable vina: -10.352

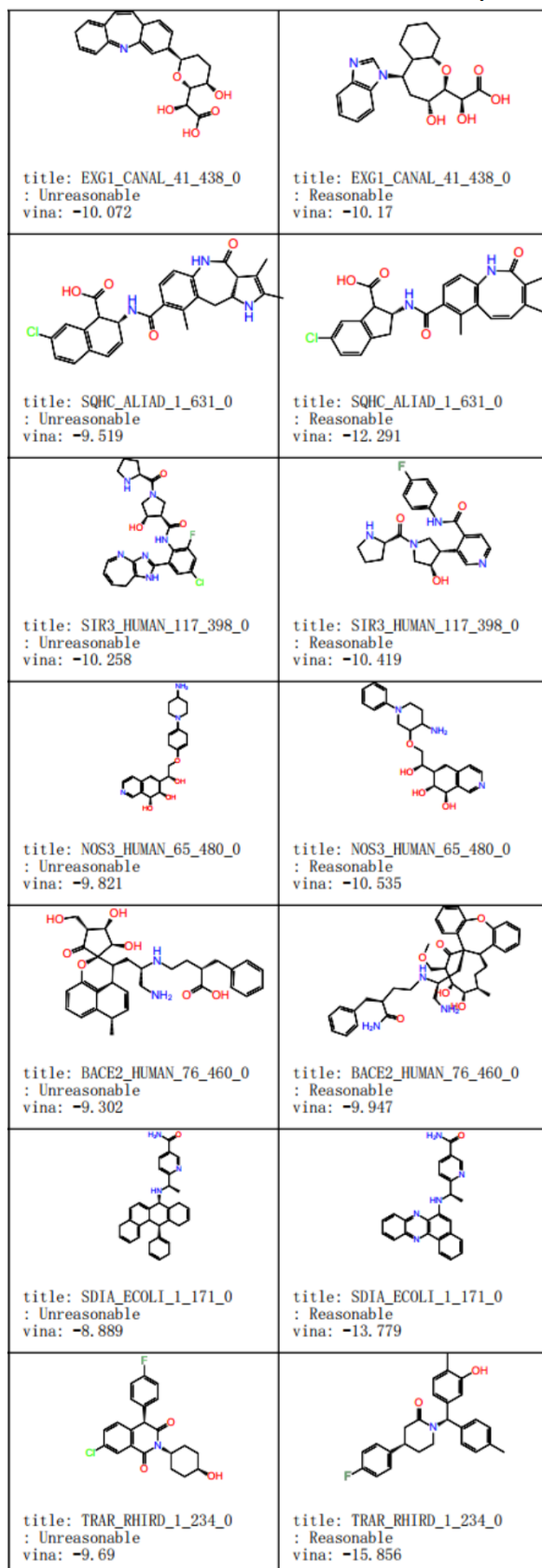
## Supporting molecule

## CIDD output

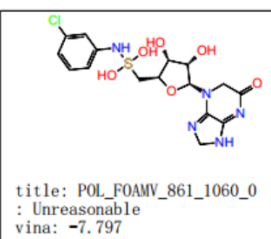


## Supporting molecule

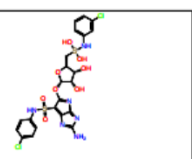
## CIDD output



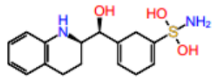
## Supporting molecule



## CIDD output



## Supporting molecule



## CIDD output

